Ecological Engineering 109 (2017) 101–118

Contents lists available at ScienceDirect

Ecological Engineering

journal homepage: www.elsevier.com/locate/ecoleng

Research Paper

Experimental study on the effect of turbulence in pipelines on the mortality of *Limnoperna fortunei* veligers

Chendi Zhang[a], Mengzhen Xu[a,*], Zhaoyin Wang[a], Wei Liu[a], Dandan Yu[b]

[a] State Key Laboratory of Hydroscience and Engineering, Tsinghua University, Beijing 100084, China
[b] State Key Laboratory of Hydrology-Water Resources and Hydraulic Engineering, Hohai University, Nanjing 210098, China

ARTICLE INFO

Keywords:
Limnoperna fortunei
Pipeline
Turbulence-generating material
High frequency turbulence
Mortality
Kolmogorov scale

ABSTRACT

Golden mussels (*Limnoperna fortunei*), an invasive species of Mytilidae, settle on the inside surfaces of water pipelines with high density, often resulting in heavy biofouling and pipe clogging. The species invades pipelines during its planktonic veliger stage, which is apt to be killed by high frequency turbulence produced by turbulence-generating materials (TGMs), such as pore plates, which can be installed inside the pipelines. However, little is known about the influence of different types of TGMs on the pipeline hydraulics and veliger-killing mechanism. An experimental study was conducted to investigate the veliger-killing mechanism and pick out the most efficient TGM for veliger killing and prevention of golden mussel invasion in pipelines. Four types of TGMs, plates with hole diameters of 3 mm (PP3) and 6 mm (PP6) and wires with mesh spacings of 3 mm (WM3) and 2 mm (WM2), were installed in a 12.6 m-long experimental pipeline with sparse (space between two PP or WM = 50 cm) and intensive (space = 25 cm) layouts. The flow field downstream of the TGMs was measured by an Acoustic Doppler Velocimeter (ADV). The experimental results revealed that the TGMs caused a short disturbance both transversely and longitudinally downstream. The disturbance was significant for PP6 and weakened for the intensive layout. The WMs exhibited little influence on the discharge capacity of the pipe and enhanced the downstream flow velocity within a short distance for the intensive layout. The distribution of the downstream turbulence intensity of the TGMs presented a uniform transverse pattern except for WM2. The TGMs enlarged the frequency of the dissipation range in the energy spectra for turbulence and consequently reduced the length scale of the dissipative eddies, i.e. the Kolmogorov length scale. A positive relation was identified between the downstream $(d^*)_{max}$ (the maximum ratio of the veliger body length to the Kolmogorov length) and the killing rate (increase of the veliger mortality rate after treated by the turbulence generated in the experimental pipeline). The test results indicated that the veliger community would be heavily damaged when the dissipation range (the Kolmogorov scale) had a similar or smaller length scale than the veliger body length. Therefore, $(d^*)_{max}$ was considered to be a representative indicator for the evaluation of the killing effect of TGMs. The TGM could be considered to have high and steady killing capacity if $(d^*)_{max} > 1$. PP6 with a sparse layout is recommended for the control of golden mussel veligers considering both the killing efficiency and economic efficiency.

1. Introduction

Golden mussel (*Limnoperna fortunei*, Dunker, 1856), is a freshwater invasive species of Mytilidae. The species has extremely high environmental adaptability, which allows it to survive in a very wide range of aquatic habitats: temperature range = 0–35 °C, flow velocity range = 0.1–2.0 m/s, water depth range = 0.1–40.0 m and dissolved oxygen range = 0.2–11.3 mg/L (Darrigran et al., 2011, 2012). Golden mussels were first found in the Pearl River basin in China (Dunker, 1856) and later spread to Hong Kong (Morton, 1977) and the Yangtze River basin (Liu et al., 1979) through water transfer projects or shipping. It was even recently found in the Shisanling pumped storage power station in Beijing (Ye et al., 2011). Golden mussels enter water transfer facilities during their planktonic veliger stages (Darrigran et al., 2007). The adults have golden yellow or dark brown shells (Xu, 2012) and are able to aggregate in high density with their byssal threads attaching to the substrate (Montalto and Rojas Molina, 2014). The invasion and mass aggregation of golden mussels usually cause serious biofouling to water transfer projects and hydraulic structures by (1) increasing the roughness of the pipe wall and decreasing flow capacity,

* Corresponding author.
E-mail addresses: xumz07@gmail.com, mzxu@tsinghua.edu.cn (M. Xu).

http://dx.doi.org/10.1016/j.ecoleng.2017.08.024
Received 14 March 2016; Received in revised form 21 August 2017; Accepted 22 August 2017
Available online 19 September 2017
0925-8574/

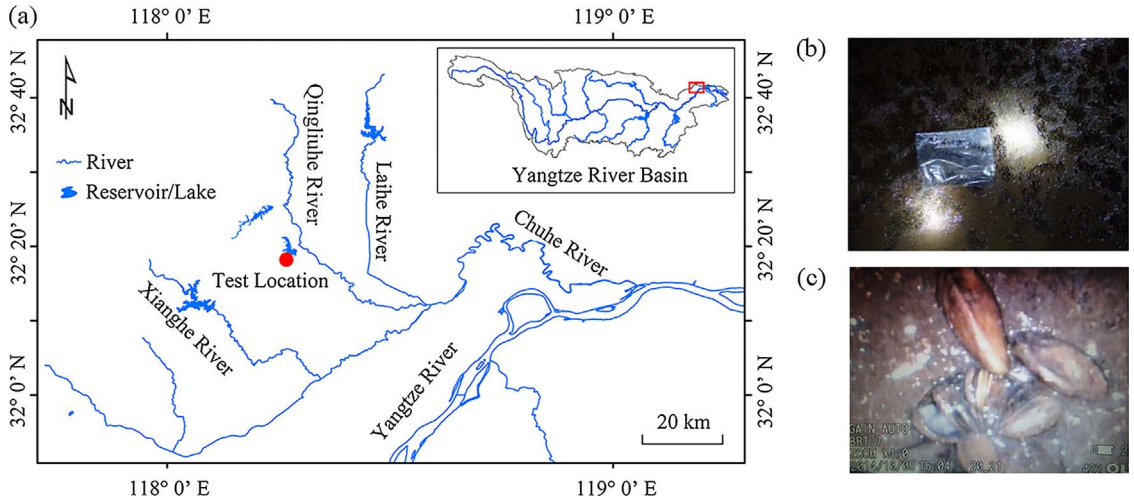

Fig. 1. (a) Experimental location; (b) Golden mussel biofouling on underground water transfer tunnels; and (c) Golden mussels in cooling pipelines with a diameter of 54 mm.

even leading to pipe clogging (Group of Pipeline Study, 1973); (2) corroding the concrete wall and lowering the concrete strength (Perez et al., 2003); (3) consuming dissolved oxygen in the water and excreting ammonia nitrogen which results in water quality degradation when the larvae are alive, and leading to water pollution due to saprogens living on their corpses (Darrigran, 2002); and (4) causing great safety hazard and economic loss by jamming structures such as biological membranes, coolers, pumps, sluice gates, etc. (Ricciardi, 1998).

Researchers and engineers around the world have carried out numerous studies to investigate strategies for the control of golden mussel invasions. Common engineering methods to remove golden mussels attached to surfaces are high-pressure water blasting and scraping manually or by machine (Xu et al., 2009). Interception by filter screens, ultraviolet radiation, thermal treatment, electric shock, chemicals, etc. have all been attempted (Fushoku and Bumon, 1999; Xu et al., 2009; Pereyra et al., 2011, 2012), but the disadvantages of these methods such as high cost, poor operability, and potential environmental pollution have limited their applications (McEnnulty et al., 2001; Xu, 2012). Intensive invasion by golden mussels has been found to occur mainly during the stage of planktonic veligers (Darrigran et al., 2007; Xu et al., 2015b). Therefore, attention has been drawn to the destruction of planktonic veligers. Based on field investigation and flume experiments focusing on the veligers, Xu et al. (2015a) established an integrated ecological prevention method which involved eliminating main sources, attracting attachment on proper materials, utilizing a settling pool, death by high-frequency turbulence, and predation by fish. This method successfully controlled the invasion and biofouling by golden mussels in a model water transfer tunnel.

Rehmann et al. (2003) employed an aerating pump to generate high-frequency turbulence in the water when trying to find a way to prevent zebra mussel invasions. It was found in the experiment that the mortality of zebra mussel veligers would increase once the Kolmogorov scale of turbulent eddies approached their body lengths. Since zebra mussels belong to the same family as golden mussels, the two species mostly share the same biological and ecological characteristics (Morton, 1979; Ricciardi, 1998; Karatayev et al., 2007). Inspired by Rehmann's attempt, Xu et al. (2012) tested introducing airflows into the water using an aerating pump and found that the mortality of golden mussel veligers also increased significantly. The veligers exhibited death modes such as breakage of the shells and release of the tissues, which implied that high-frequency turbulence was effective in killing golden mussel veligers (Jessopp, 2007). Considering economic efficiency for engineering application, Xu (2012) designed a high-frequency turbulence generating system by installing pore plates at different cross sections in a pipeline, which was proven to be effective in enhancing the mortality of golden mussel veligers. The installation of pore plates has little influence on water quality but high practical potential for engineering projects with large hydraulic head (Xu, 2012).

Xu (2012) tested the killing effect of the turbulence generated by pore plates with hole diameters of 10 mm and plate-to-plate spacing of 50 cm installed in an experimental pipeline. However, other types of turbulence generating materials (TGMs) and layouts were not studied in Xu's trial and the hydraulic characteristics of the generated turbulence was not explored. The mechanism of veliger mortality resulting from turbulence in pipelines remained poorly understood. The purpose of the present study was to reveal the hydraulic characteristics of the turbulence field downstream of the TGM, and to link the hydraulic characteristics and killing effects for better understanding the killing mechanism of the TGM. A hypothesis was proposed for this study that the damage to the veligers was triggered by turbulent eddies with a dissipation range of similar or smaller length scale than the veliger size, based on the results of Rehmann et al. (2003) and Xu (2012). Four types of TGMs were installed inside the experimental pipeline with sparse and intensive plate-to-plate layouts. The characteristics of the downstream flow fields of the TGMs were measured, and the turbulence intensity and spectrum were analyzed. The mortality tests for golden mussel veligers were done afterwards to examine the enhancement of the veliger death rate after the water flowed through the pipeline with TGMs. The effect of treatment time of turbulence generated by the TGMs on veligers was also explored by conducting circular tests (with a certain water volume circulating in the pipeline). The developmental stages, death modes, and changes in the death rate of the veligers were analyzed. Lastly, the hypothesis for the killing mechanism was validated by the experimental results.

2. Study location and methods

2.1. Experiment location

The pipeline turbulence experiment was conducted on the bank of the downstream reservoir of the Langyashan pumped storage power station (PSP), which is located in the southern suburb of Chuzhou city, Anhui Province, in the lower Yangtze River basin (Fig. 1a). The Langyashan PSP functions for peak power regulation in the East China power network and its lower reservoir serves as the drinking water source for Chuzhou city. However, severe golden mussel biofouling has caused a threat to the proper functioning of the station. Golden mussels have thrived on the walls of the water delivery pipelines (Fig. 1b). Especially, the cooling pipelines with a diameter of 54 mm can easily get clogged by the multilayer attachment of adult golden mussels whose

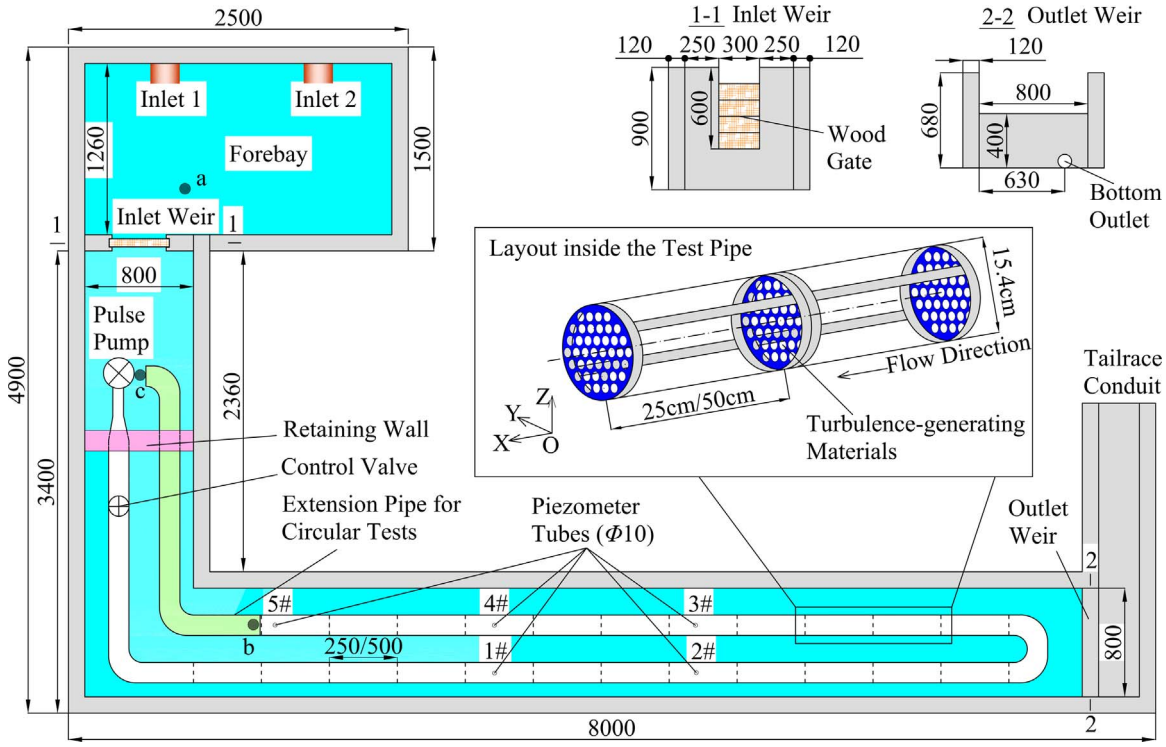

Fig. 2. Plan view schematic of the experimental system set-up and interior layout (units: mm). Points a, b and c refer to locations for golden mussel larva sampling. Holes 1#–5# were for the piezometer tubes.

shell length usually reaches 20 mm (Fig. 1c), potentially leading to a sudden stop of the generators and endangering the operation of the station. Given that the reservoir is the local drinking water source, chemical controlling strategies are not applicable. There is about 100 m water head between the upper and lower reservoirs, supplying large geopotential energy, which can be made use of if TGMs are installed in the pipelines to kill golden mussel veligers.

2.2. Experimental system

The experimental system consists of a forebay, an experimental flume, and a tailrace conduit, with all parts built with bricks and cement. Two submersible pumps (the lift and discharge were 7 m and 60 m^3/h for one of the pumps, and 15 m and 25 m^3/h for the other) were installed in the downstream reservoir and kept pumping water to the forebay (2 m long and 1.26 m wide with a water depth of 0.90 m when it was full). The experimental flume was 0.80 m wide and 0.68 m high. A gate slot was set up at the inlet weir of the flume with several wood blocks of the same size to control the inflow discharge (Section 1-1 in Fig. 2). An overflow weir was constructed at the outlet of the flume to keep the maximum water depth at 0.385 m and a bottom outlet in the weir was used to empty the flume (Section 2-2 in Fig. 2).

An experimental pipeline of UPVC (Unplasticized Polyvinyl Chloride) material with an external diameter of 16 cm and an internal diameter of 15.4 cm was placed at the bottom of the experimental flume, and was connected to a pulse pump (lift of 15 m and discharge of 25 m^3/h) at the inlet. The 12.6 m-long pipeline consisted of 6 pipe segments and one 180° fold-back connection.

The entire pipeline guaranteed sufficient pipe length for the development of smooth and steady flow at the outlet of the test pipeline and for enough TGMs to be installed for the veliger-killing tests. Two kinds of tests were performed in this study: direct killing test and circular killing test. The water from the forebay at a discharge of 0.018 m^3/s flowed through the pipeline only once in the direct killing tests while the inlet gate was closed and the circulated water volume was kept at 0.53 m^3 (involving water in the pipeline and water between the inlet weir and the retaining wall) in the circular killing tests. During the hydraulic measurements and direct killing tests, a 0.4 m-long extension pipe was connected to the outlet of the pipeline to keep the flow regime at the outlet as pipe flow instead of jet flow. When the circular tests were performed, a 2.1 m-long "L"-shaped pipe segment (the green one in Fig. 2) was installed at the pipeline outlet to make the pipeline outlet closer to the pulse pump. Since a gap still remained between the extension pipe outlet and the intake of the pulse pump, a waterproof retaining wall with the same height as the flume wall was installed to isolate the water volume around the pulse pump.

Five holes with a diameter of 1 cm were drilled in the test pipeline (1# ~ 5# in Fig. 2) for the connection with piezometer tubes. All the piezometer tubes were fixed on a 4.6 m-high calibration board.

2.3. Turbulence-generating materials

Based on the previous tests of Xu (2012), pore plates (PPs) are applicable for generating high-frequency turbulence, if installed perpendicular to the flow direction in the pipeline, because alternate jets and wakes are produced downstream (Yan et al., 2005). Two models of PPs with holes smaller than those applied in Xu's experiment were selected as the TGMs in this study (Table 1, Fig. 3). In addition, two models of wire mesh (WM) materials were also tested (Table 1, Fig. 3). All the PPs or WMs were fixed in 3 mm-thin galvanized frames and then put into the pipeline (as shown in the inner layout of the pipeline in Fig. 2).

2.4. Hydraulic measurements

Flow velocity and turbulence characteristics were measured with a Vectrino Acoustic Doppler Velocimeter (ADV) manufactured by Nortek, Norway. The measurement range of the flow velocity is −4 to 4 m/s. The maximum sampling frequency of the ADV is 200 Hz.

The ADV was installed in a bracket, allowing it to move vertically. The bracket was fixed on a slider with a 1.1 m-long rail. The resolution of the depth gauge and the horizontal gauge on the rail was 0.1 mm and 1 mm, respectively. The ADV probe location was defined by the two

Table 1
Turbulence-generating material (TGM) parameters.

Code	Type	Hole shape	Aperture/mm	Distance between neighboring holes/mm	Porosity/%
PP3	Pore Plate	Round	3	1.96	0.36
PP6	Pore Plate	Round	6	2.34	0.52
WM2	Wire Mesh	Rectangular	2	0.42	0.68
WM3	Wire Mesh	Rectangular	3	0.91	0.64

Porosity = Pore area/total area.

gauges. The probe was oriented vertically and the measuring sections were vertical to the flow direction (Fig. 4a). Given that the probe was 5 cm away from the sampling location to minimize its disturbance to water (Garcia et al., 2005) and that the probe itself occupied a certain space, the measuring points were assigned on only one half side of the measuring section on two measuring lines, H and V (Fig. 4b and c). The sampling time at each measuring point was 60 s at 200 Hz to guarantee the volume of each measurement is larger than 10^5, which exceeds the threshold of 5000 as suggested by Chanson et al. (2007) for the analysis of the first and second statistical moment.

2.5. Experimental procedure

2.5.1. Hydraulic measurement

Based on the experimental results of Xu (2012), 50 cm was selected as the TGM spacing for the sparse layout and 25 cm was selected for the intensive layout. The last TGM was fixed during the measurements, other TGMs were added or removed upstream for trials with different TGM numbers (Fig. 4d). All the hydraulic measurements should have been done with the entire experimental pipeline installed with TGMs. However, to avoid the damage due to frequent detachments of pipe segments during a large number of tests, most tests were conducted within the outlet pipe segment (2.5 m long) installed with TGMs for simplification. In these test, the total lengths of the TGM frames were the same in the sparse and intensive layouts for comparison purposes, e.g., 5 TGMs arranged for the intensive layout and 3 TGMs for the sparse layout. In order to verify the equivalence of the simplification, 25 TGMs were installed in the entire pipeline at spacing of 50 cm or from the pipeline outlet to the middle of the pipeline at spacing of 25 cm. When measuring the downstream flow fields of the TGMs, the measuring sections were set at a Measuring Distance (*MD*) of 2.5, 5.0, 10.0, 17.0, 25.0, and 50.0 cm for the sparse layout and at *MD* of 2.5, 5.0, 10.0, 17.0, and 25.0 cm for the intensive layout (Fig. 4d).

2.5.2. Veliger-killing test

The killing tests were conducted after the golden mussel veliger density in the reservoir had reached 500/m^3 for several days, which was sufficient for reliable death rate comparison and larval developmental stage analysis. The four types of TGMs installed sparsely and intensively were all applied in the killing tests. For each test, 25 TGMs were installed in the experimental pipeline. Water samples were taken both before and after treatment by the TGMs. The pre-treatment samples were taken at point “a” in the forebay (Fig. 2), while the post-treatment samples were taken at points “b” and “c” (Fig. 2) for direct killing tests and circular killing tests, respectively. During the direct killing tests, water samples were taken at “a” and “b” at almost the same time. During the circular killing tests, water samples were taken at “a” and “c” simultaneously at the 1st minute after switching on the pulse pump. Then water samples were only taken at “c” at the 5th, 10th, and 15th minute. For each water sample, 80 or 120 L of water was taken by a siphon and filtered through a plankton net with meshes of 50 μm and the filtered liquid was collected in sampling bottles (Xu et al., 2015b). After about an hour for settling, the concentrated samples were extracted and observed under a microscope-camera system (SmartV Camera & MIVNT Image Analysis Software, Yongheng Shanghai). Numbers of the living and dead larvae, developmental stages of the living larvae, and death modes of the dead were documented.

3. Data processing

Raw data from the ADV cannot be used directly for spectrum analysis because of its noise and spikes (Chanson et al., 2007). The noise mainly consists of Doppler noise which is inherent to the device (Lohrmann et al., 1994) while the spikes are generated when the phase shift between the transmitted pulse and received pulse exceeds the range of −180° to 180° (Goring and Nikora, 2002). The velocity records with signal-to-noise ratio less than 15 dB were abandoned in the de-noising process (Rusello et al., 2006) and acceleration Thresholding Method was utilized in the despiking process (Goring and Nikora, 2002) for the preprocessing of the present study.

The fluctuation components in the transient velocities are defined by:

$$u' = U - u,\ v' = V - v,\ w' = W - w \tag{1}$$

where u', v', and w' are fluctuating velocity components; U, V, and W are time-average velocities corresponding to the directions X, Y, and Z, respectively (Fig. 4); and u, v, and w are the transient velocities.

The turbulence intensity is calculated by the standard deviation of the time series of fluctuating velocities (Pope, 2000):

$$\sigma_u = \sqrt{\overline{(u')^2}} = \sqrt{\frac{1}{n}\sum_{i=1}^{n} u'^2},$$
$$\sigma_v = \sqrt{\overline{(v')^2}} = \sqrt{\frac{1}{n}\sum_{i=1}^{n} v'^2},$$
$$\sigma_w = \sqrt{\overline{(w')^2}} = \sqrt{\frac{1}{n}\sum_{i=1}^{n} w'^2} \tag{2}$$

where σ_u, σ_v, and σ_w are the standard deviations of u', v', and w', respectively; and n is the number of velocity records in each

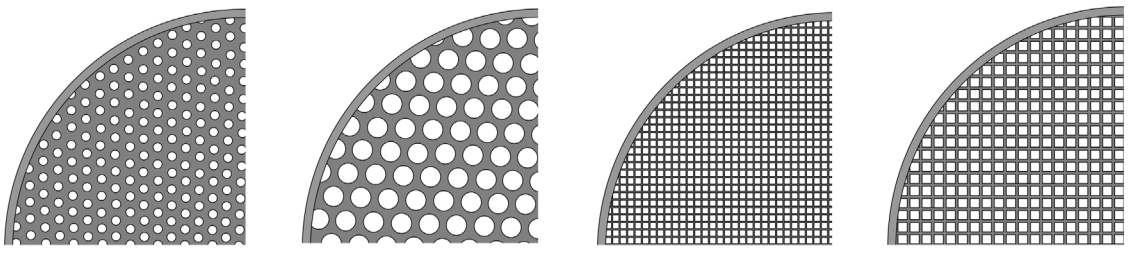

Fig. 3. The four TGMs employed in this study. Only a quarter of each TGM is shown in order to present the evaluated details of pores and meshes.

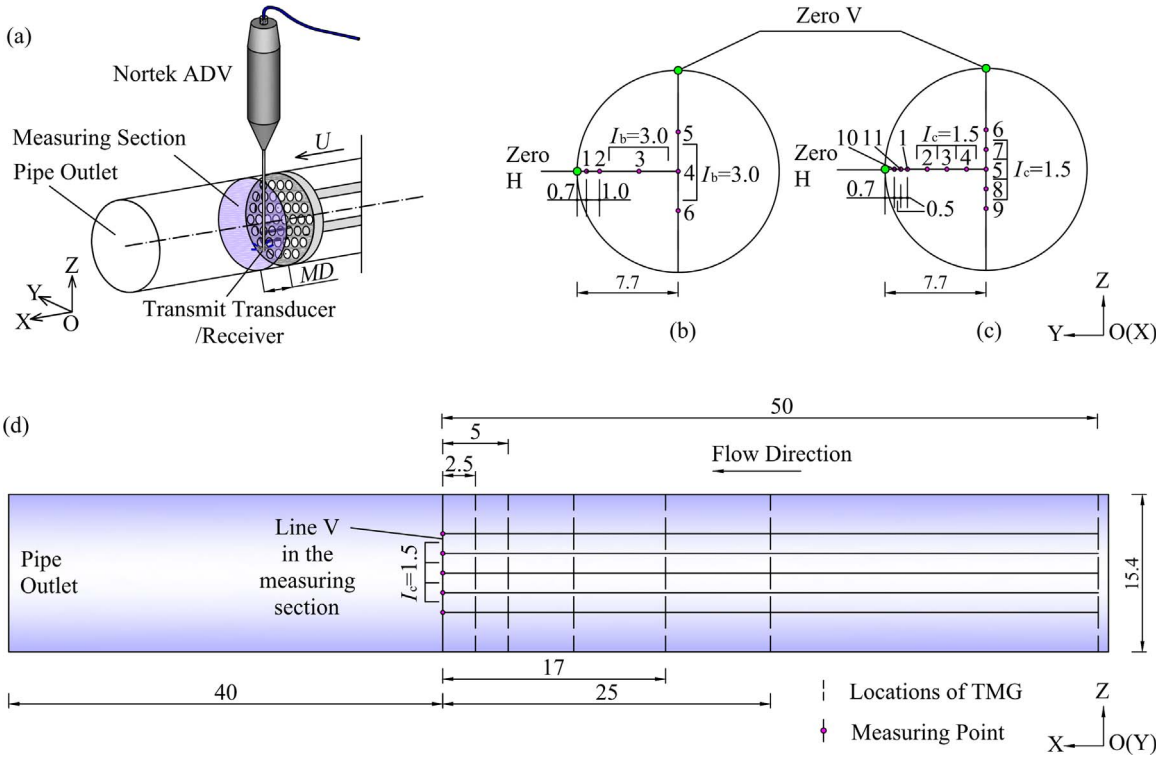

Fig. 4. (a) Schematic diagram of the ADV installation. *MD*: measuring distance, which refers to the distance between the last TGM and the measuring section; (b) Layout of 6 measurement points. I_b refers to the interval from point 2 to point 6 and I_b = 3.0 cm. (c) Layout of 11 measuring points. I_c refers to the interval from point 2 to point 9 and I_c = 1.5 cm. Most of the tests were done with the layout in (c). Zero points of all the measuring lines are marked in green points in (b) and (c); and (d) Side view of the measuring section and the last TGM. The velocity component is positive if it is in the same direction as the corresponding coordinate axis. Units are in cm. (For interpretation of the references to colour in this figure legend, the reader is referred to the web version of this article.)

measurement.

The energy spectrum was calculated using the Welch (1967) method based on Fourier Transformation (Pope, 2000):

$$E = \frac{1}{2\pi}\int_{-\infty}^{\infty} R_{uu}(t)e^{-i\omega t}dt \tag{3}$$

where $\omega = 2\pi f$ is the angular frequency; f is the frequency; and $R_{uu}(t)$ is the temporal autocorrelation function of the fluctuating velocity.

The vertical coordinate stands for the energy density after Fourier Transformation in the spectrum. The integral of E was calculated every 1 Hz to obtain the turbulent energy of each frequency, which equaled to the average energy density of every 1 Hz numerically.

4. Results

4.1. Influence of number of TGMs on the downstream flow field

As stated previously, the TGMs were only installed in the last segment of the pipeline for the measurement of the hydraulic characteristics. The feasibility of the measurement for the simplified installation was verified before it was applied in hydraulic measurements. The measurement results of WM3 at *MD* = 2.5 cm were presented as an example to illustrate the influence of the number of TGMs (set as 1, 2, 5, 6, 25) on the hydraulic features (Figs. 5 and 6). Measurements in a blank pipeline without TGMs were conducted for comparison purposes. The spectrum of the center of the measuring section was also analyzed.

The flow characteristics of line H exhibited the features of both the boundary layer and the main flow area, and the former was influenced by the TGM to a larger degree (Fig. 5). It was found that U varied in the range of 0.9-1.3 m/s and its transverse distribution insignificantly differed as the number of TGMs increased, similar to the results for pipe without TGMs. V and W both fluctuated around 0 m/s and their transverse fluctuation was stronger than that in the pipe without TGMs. The magnitude of U was 10^1-10^2 times higher than V and W, which seldom changed under different numbers of TGMs. Therefore, U remained the major component of the flow velocity under different numbers of TGMs.

The turbulence intensity (σ_u, σ_v, and σ_w) became stable when the number of TGMs reached 5 (Fig. 5). The thickness of the boundary layer in the pipeline with TGMs was about 1 cm, which was thicker than that in the pipeline without TGMs, because the edge of the TGM disturbed the water passing by. The distribution of turbulence intensity was relatively uniform transversely beyond the boundary layer. The existence of TGMs resulted in higher turbulence intensity compared to the pipeline without TGMs in all directions and the increase of turbulence intensity in the Z direction was the highest. As shown in Fig. 6, the slopes of spectra were similar in all directions and when the TGM number increased to 5, 6 and 25, the turbulent energy stayed the same. Therefore, the influence of the number of TGMs on spectrum was negligible when more than 5 TGMs were installed.

Measurement results for the other TGMs were similar: the distribution patterns of velocity and turbulence intensity rarely varied when the number of TGMs exceeded 3 for TGM to TGM spacing of 50 cm and exceeded 5 for the spacing of 25 cm. Therefore, hydraulic measurement for a simplified installation of TGMs was feasible in studying hydraulic characteristics. Since U was much larger than V and W, most of the following discussions are focused on the characteristics of U.

The inertial subrange started at high frequencies due to the small scale of the energy-containing range in this study, leaving little room in the fixed measurement range (0–200 Hz) to present the entire inertial subrange (Garcia et al., 2005). However, the starting frequency of the inertial subrange still indicated the spectrum features considering that the inertial subrange had similar slopes ($-5/3$) in the double logarithm coordinates (Pope, 2000).

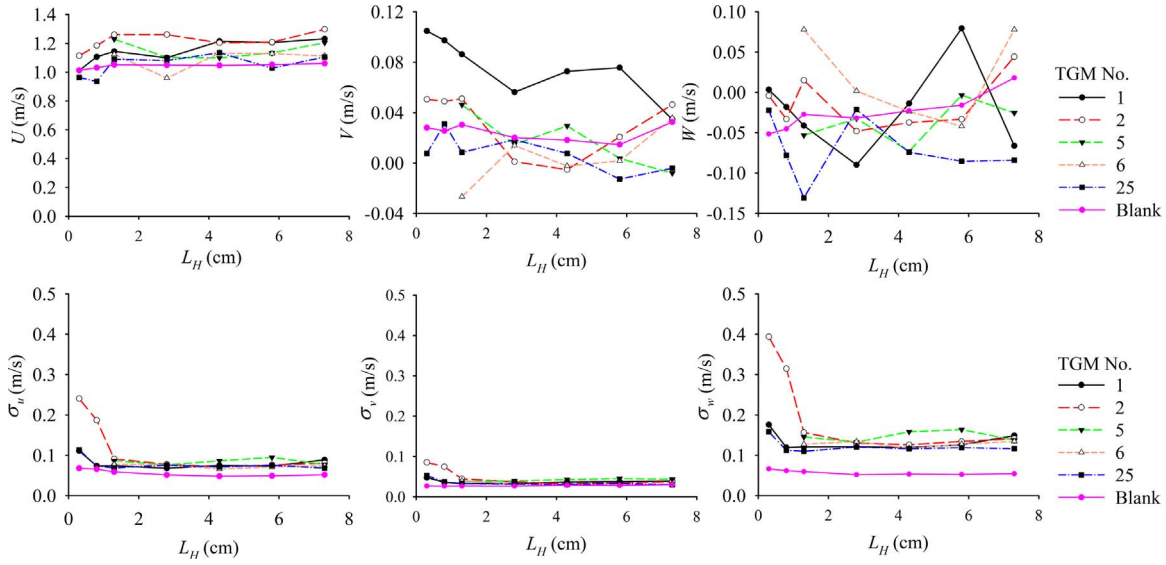

Fig. 5. Distribution of time-averaged velocity and velocity fluctuation components (X, Y, and Z directions) along line H for different numbers of WM3 (sparse layout) at MD = 2.5 cm. L_H in the figure refers to the distance from a measuring point to the zero point.

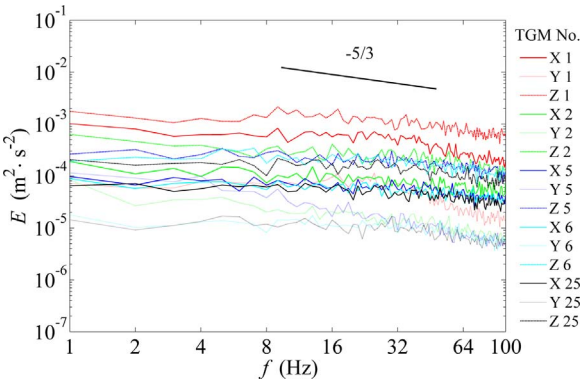

Fig. 6. Energy spectra at the centers of measuring sections for WM3 with spacing of 25 cm.

4.2. Flow velocity distribution

The measurements along line V were considered when analyzing the velocity and turbulence intensity distribution. In general, the transverse distribution of U was symmetrical as expected except that a fluctuation of U existed transversely within the MD of 5 cm (Fig. 7a), especially for PP6. The fluctuation decreased as the MD surpassed 5 cm and the transverse distribution of U tended to be the same as for the pipe without TGMs, which indicates that TGMs have significant influence on the transverse distribution of flow velocity only for a limited distance, e.g., 5 cm in this study.

Fig. 7 illustrates that the PP3 installation resulted in a decrease of flow velocity compared with the pipe without TGMs due to its small porosity (Table 1), but this TGM had a uniform transverse distribution of flow velocity. In contrast, when PP6s were installed, the flow velocity fluctuated significantly within 5 cm downstream, especially for the layout with the spacing of 50 cm, which might be attributed to the intensive jets and wakes downstream because of its large aperture and distance between neighboring holes (Table 1). The fluctuation was inhibited when the intensive layout of TGMs was employed (Fig. 7b). As for WM2 and WM3, both resulted in a relatively even distribution of flow velocity and similar velocity magnitude as that in the pipeline without TGMs, indicating that the WMs of different apertures hardly had any influence on the flow capacity of the pipe. However, with the spacing of 25 cm, the velocity increased sharply immediately after the water went through the WMs while it decreased to the same level as that in the pipe without TGMs as water flowed downstream for over 5 cm. This velocity increase was more distinct for WM2, implying that smaller pore sizes were more effective in intensifying jets of WMs when the spacing was reduced.

The arithmetic mean of velocity along line V (U_{mean}) at each measuring section was calculated as a reference for the longitudinal distribution of flow velocity downstream from the TGM. It was found that U_{mean} was larger in the downstream area close to the TGM (Fig. 8a). This is related to the reduction of the effective area for the water passage at the TGM, leading to an increase of upstream pressure energy and the resulting transformation of this energy into kinetic energy in the area downstream of the TGM. As shown in Fig. 8a, U_{mean} decreased as water flowed away from the last PP and came to its minimum before the next PP because the resistance from the PP initiated the transformation from kinetic energy to pressure energy. The U_{mean} for WMs kept decreasing after water flowed through a WM but reached an almost constant level beyond MD = 10 cm, which was different from PPs because of the WMs' lower resistance. Another difference between PPs and WMs was that U_{mean} increased as the aperture of PP became larger but stayed almost the same with larger aperture of WM. In accordance with the findings shown in Fig. 7, the transverse fluctuation, which only lasted for less than 10 cm, was relatively large after the water just passed through the TGM (Fig. 8b).

4.3. Turbulence characteristics

4.3.1. Distribution of turbulence intensity

Given that the turbulence intensity in the Z direction was the largest in magnitude and most intensively influenced by the TGMs in all three directions (Fig. 5) and experienced the least noise during the measurements (Hussein et al., 1994; Voulgaris and Trowbridge, 1998), the data for the Z direction were utilized in the turbulence analysis.

The downstream distribution of the turbulence intensity with the PP installation shows a banded feature with intensity decreasing along the pipeline in a transversely uniform way. For WMs, the turbulence intensity also decreased along the pipeline but did not show a distinct banded distribution because the turbulence intensity around the boundary layer exceeded that in the central area (Fig. 9), particularly for WM2. The turbulence intensity in the majority of the downstream area of WM2 was smaller than that of the pipe without TGMs except for the area close to the TGM (within 3 cm) (Fig. 10). Consequently, the

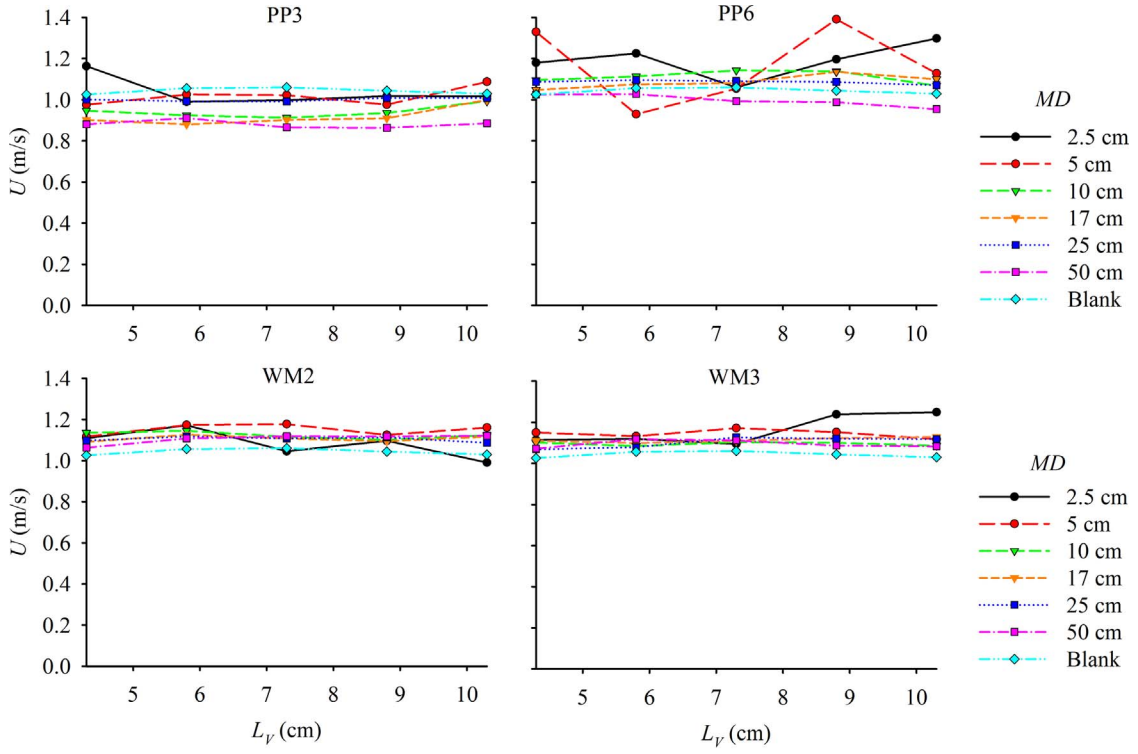

(a) Spacing of 50 cm

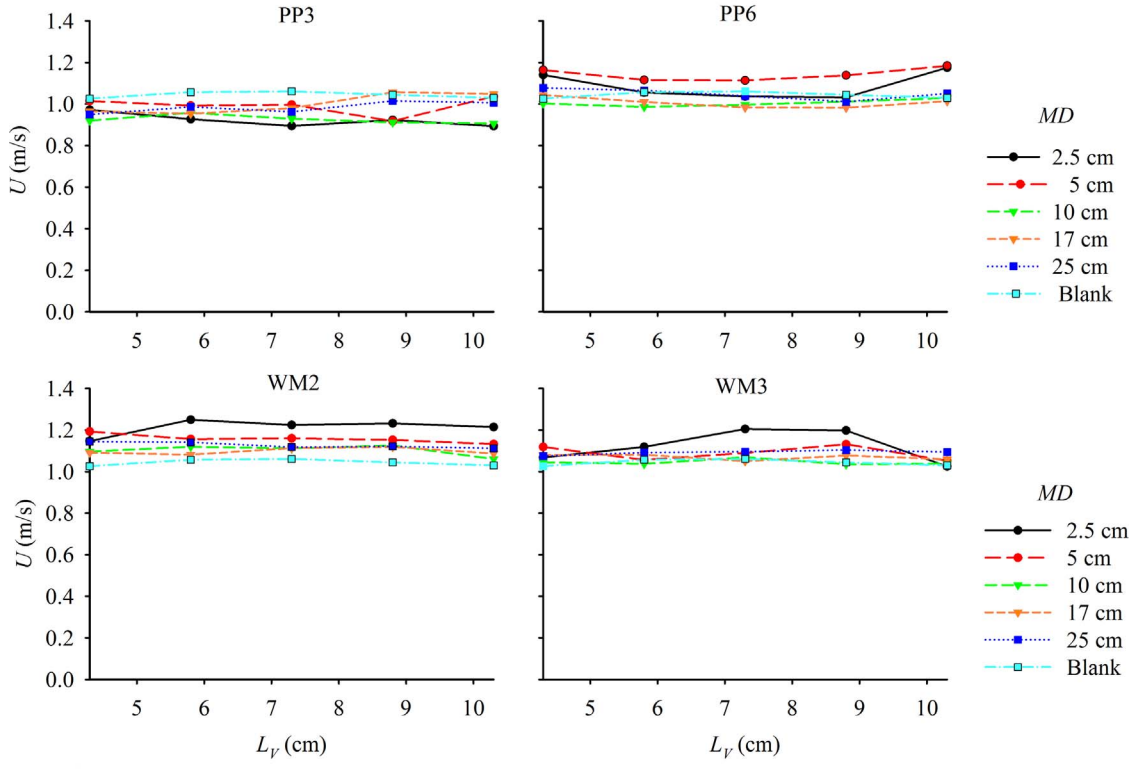

(b) Spacing of 25 cm

Fig. 7. Distribution of U for each TGM with (a) the spacing of 50 cm and (b) the spacing of 25 cm. L_V refers to the distance from a measuring point to the zero point of line V.

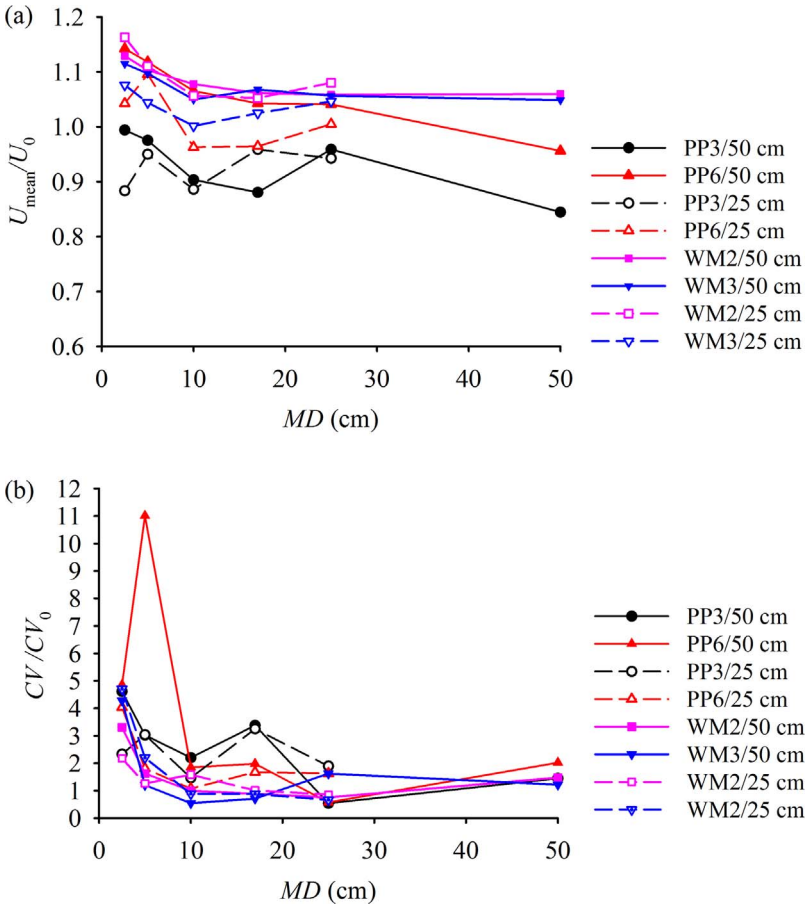

Fig. 8. (a) Longitudinal distribution of U_{mean}/U_0; (b) Longitudinal distribution of CV/CV_0. U_{mean} and U_0 are the arithmetic mean of the velocities measured in line V with TGMs and without TGMs, respectively. CV_0 is the coefficient of variation in the pipe without TGMs. The length behind the "/" refers to the spacing of the TGMs. CV and CV_0 refer to the coefficient of variation of the velocities in line V when TGMs are installed and when they are not installed, respectively.

turbulence induced by the pipe wall and TGM bracket was not negligible or even stronger than that in the main flow area and the transverse distribution was not uniform. The general downstream turbulence intensity of WM3 was higher than that of WM2 and was close to that for the pipe without TGMs, therefore, there was no distinct gap in the turbulence intensity between the boundary layer and the central area and the banded pattern was obtained. As for the PPs, the absolute value of the downstream turbulence intensity was largely enhanced by the TGMs and the effects of the boundary layer was negligible. The downstream turbulence intensity of the PPs exceeded that of the WMs to a large extent (Fig. 10), e.g., the maximum of the downstream turbulence intensity of PP6 was over 12 times stronger than that of WM2.

It appeared in the longitudinal profile of the turbulence intensity that the area affected by the TGMs was spatially limited. The largest value occurred within the 5 cm-long area downstream of the TGMs and the intensity decreased as the water flowed farther downstream, reaching a constant value close to that for the pipeline without TGMs after 10 cm away from the TGMs (Fig. 10).

4.3.2. Energy spectrum

To explore the frequency composition of turbulence generated by the TGMs, the energy spectrum of W at the center of each measuring section was calculated and compared with its counterpart in the pipeline without TGMs. The spectra presented significant differences between the different types of TGMs for both the sparse and intensive layouts (Fig. 11). For the pipeline without TGMs, the low-frequency range (< 20 Hz) obtained applying with the Kolmogorov hypothesis (Pope, 2000) lay in the inertial subrange. For the higher frequency range (> 20 Hz), the slope increased and the spectrum dropped into the transition and dissipation range. For the PPs, the spectra had a relatively small slope (even close to 0 for PP6) when the water immediately past the PP, and, thus, the starting point of the inertial subrange substantially increased, even approaching the extremity of the measurement range for PP6. The inertial subrange started from the lower frequency conditions when the water flowed farther than 5 cm away from the PPs. The frequency of the inertial subrange was higher with the WM installation than that for the pipe without TGMs but lower than that for the PPs.

The turbulent energy of the high-frequency range (> 50 Hz) for the PPs was enhanced to a large extent in comparison to the pipeline without TGMs: the increase was over 10^3 times for PP6 and 10^2 times for PP3 (within the measurement range) than the corresponding values for the pipe without TGMs. The turbulent energy for the WMs also increased when the water just passed the TGM, but to a much smaller degree compared with that for the PPs. The largest increase for WM3 was 10^1 times higher than that for the pipe without TGMs. In contrast, there was a decrease in the turbulent energy of the low-frequency range (< 20 Hz) for WMs. The majority of the area downstream of WM2 had lower turbulent energy than that in the pipe without TGMs, which would explain why the downstream turbulence intensity was lower (Fig. 10). Such a decrease might result from the breaking down of large scale eddies due to small apertures of the WMs and the relatively high dissipation rate of the broken eddies with small scales (Mohamed and LaRue, 1990). No significant influence of the intensive layout was observed on the spectra.

4.4. Hydraulic head loss

Hydraulic head losses along the pipeline were recorded and are listed in Table 2 (the floor was the base level). It was found that the average hydraulic head loss of each PP was substantially larger than its counterpart for each WM, indicating that the PPs provided a higher

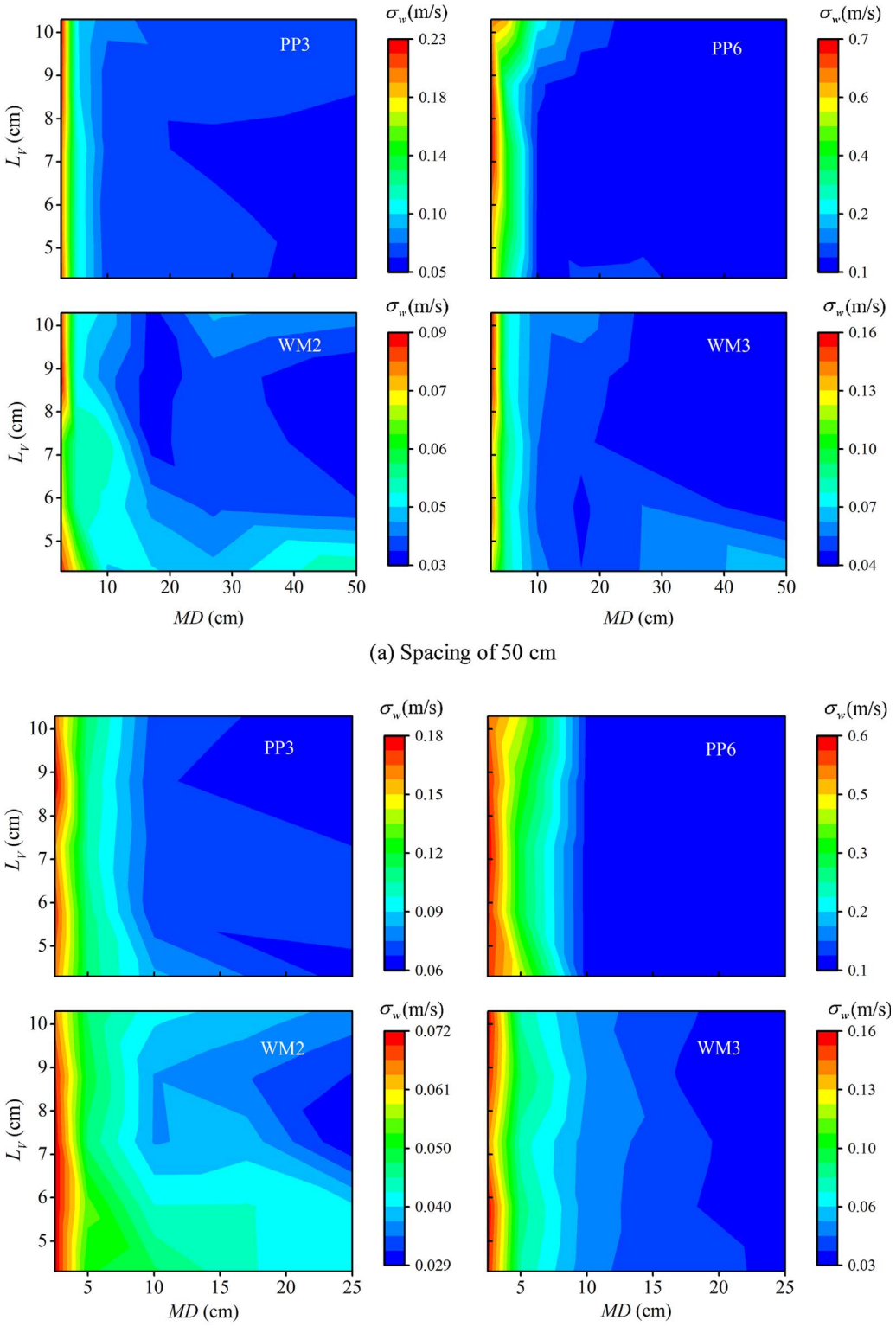

Fig. 9. Distribution of turbulence intensity for the TGM layouts with spacing of (a) 50 cm and (b) 25 cm.

resistance to the flow although it greatly enhanced the turbulence intensity. The PP materials, thus, had a disadvantage with respect to economic efficiency. The ranking from the largest hydraulic head loss per TGM to the smallest was: PP3 > PP6 > WM3 > WM2. Another finding was that the intensive layout did not significantly increase the hydraulic head losses. This finding was supported by the average hydraulic head loss calculated using the data of the entire experimental pipeline and that of each pipe segment (the average hydraulic head loss between 3# and 4# with 6 mm PP/25 cm was abnormal and was not included in the analysis).

4.5. Killing tests

4.5.1. Developmental stages and death modes of golden mussel veligers

The golden mussel larvae experiences different planktonic stages in the water until it develops into a juvenile shellfish (Cataldo, 2015; Xu

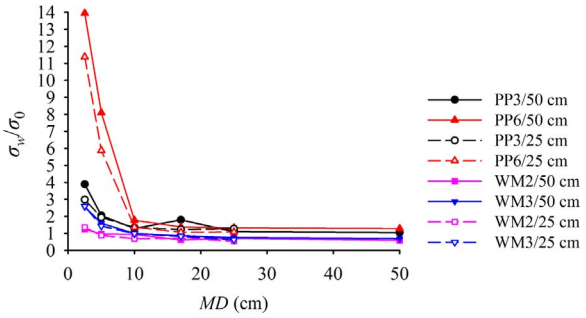

Fig. 10. Longitudinal distribution of σ_w/σ_0. σ_w and σ_0 refer to the turbulence intensity in the Z direction at the measuring section center with the TGMs and without the TGMs, respectively.

et al., 2015b). Four planktonic veliger stages were found in this study: D-shape veliger, Umboned veliger, pediveliger and plantigrade veliger (Fig. 12). Although the mobility of plantigrade veligers is improved compare to umboned veligers and pediveligers because of the development of a muscular and adhesive foot (Cataldo, 2015), their swimming velocity is still negligible compared to the flow velocity of about 1 m/s in the main flow area (Xu, 2012).

The percentages of veligers in each developmental stage fluctuated during the test period (Fig. 13) due to the differences of initial veliger density, killing rate and density of live veligers after treatment by the TGMs. However, it was obvious that umboned veligers were dominant in almost all the tests, accounting for 75.9% on average. Pediveliger ranked the second most common stage with an average percentage of 16.1%. The average percentage of plantigrade veligers and D-shape veligers was 7.1% and 0.9%, respectively. The killing tests were performed from June 20th through July 10th, 2015. The increase in percentages of pediveligers and plantigrade veligers implies the continual development of veligers over this period. However, the total percentage of umboned veligers and pediveligers remained relatively stable (70.6-100%) in all tests. Since umboned veligers and pediveligers have similar body length, which was the most important variable considered in the following analysis, the development of veligers within the test period could be ignored.

The living status of the veligers was examined after treatment by the TGMs (Fig. 14). Three death modes of veligers were found: (a) tissues of the veligers were broken and released out from the shells; (b) empty shells because all the tissues were released; and (c) the shells were damaged. These death modes indicated that physical damage occurred to the veligers due to high shear stress and turbulence (Horvath and Lamberti, 1999; Jessopp, 2007). The death modes were the same as those observed in the killing experiments with high-frequency turbulence generated by aerating pumps (Xu et al., 2015a). Therefore, it was reasonable to assume that the two experimental conditions might share the same mechanism for killing golden mussel veligers, i.e. the shear stress produced by the eddies with similar scales as the veligers could kill the veligers.

4.5.2. Direct killing test

The death rate of golden mussel veligers at sampling point “a” in the forebay was used as the control and the increase of the death rate from “a” to “b” was defined as the killing rate of the veligers. As listed in Table 3, the killing rate of PP6 was the highest in both layouts. The killing rate of PP6 was more stable under the intensive layout than under the sparse layout, which might be attributed to the more uniform transverse distribution of flow velocity under the intensive layout. The killing rate of PP3 was fair under the sparse layout but dropped distinctly under the intensive layout, owing to the decrease of flow velocity in the main flow to less than 0.9 m/s (Fig. 8a), which is consistent with the finding that only if the average velocity exceeded 0.9 m/s could the PP10 (aperture = 10 mm) work effectively in veliger-killing (Xu, 2013). Therefore, the flow capacity of the TGMs affects their killing ability. The WMs had larger flow capacities but even lower killing rates than PP6, illustrating that the turbulence intensity was

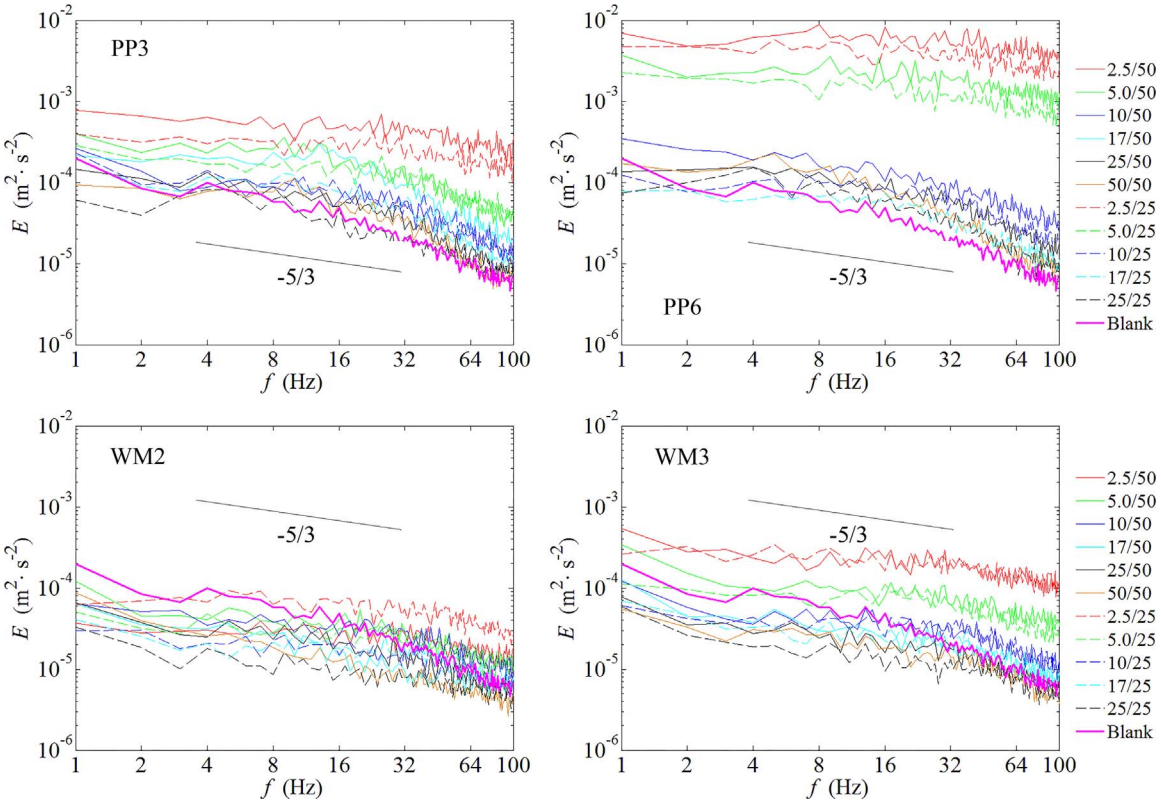

Fig. 11. Energy spectra of the center of the measuring sections at different *MDs*. X/Y refers to the situation that the *MD* is X cm and the spacing of TGMs is Y cm.

Table 2
Hydraulic head along the test pipeline.

TGM	*AP*/m	Spacing/cm	h_1/cm	h_2/cm	h_3/cm	h_4/cm	h_5/cm	$\triangle h_{1-5}$/cm	$\triangle h_{1-2}$/cm	$\triangle h_{2-3}$/cm	$\triangle h_{3-4}$/cm	$\triangle h_{4-5}$/cm
PP3	3	50	–	418.8	216.0	138.5	64.5	22.1	–	20.3	25.8	24.7
PP3	3	50	–	429.0	221.0	123.0	68.0	22.6	–	20.8	32.7	18.3
PP3	3	25	–	–	310.0	204.0	58.7	20.9	–	–	17.7	24.2
PP3	3	25	–	–	347.0	233.0	60.0	23.9	–	–	19.0	28.8
PP6	6	50	373.0	323.0	161.0	111.4	55.5	16.7	16.7	16.2	16.5	18.6
PP6	6	50	371.9	318.0	163.0	112.4	55.2	16.7	18.0	15.5	16.8	19.1
PP6	6	25	460.0	431.0	201.0	186.0	58.5	15.5	–	19.2	2.5	21.3
WM2	2	50	129.5	116.6	71.7	58.8	41.2	4.7	4.3	4.5	4.3	5.9
WM22	2	50	142.2	124.8	75.6	45.2	42.4	5.3	5.8	4.9	6.8	4.3
WM2	2	25	158.8	157.9	109.0	76.0	43.0	4.8	–	4.1	5.5	5.5
WM2	2	25	216.0	215.0	120.0	90.0	44.0	7.1	–	7.9	5.0	7.7
WM3	3	50	171.0	152.5	94.5	76.0	47.0	6.5	6.2	5.8	6.2	9.7
WM3	3	50	168.4	152.0	93.2	74.1	43.9	6.6	5.5	5.9	6.4	10.1
WM3	3	25	183.0	182.5	124.0	92.0	42.2	5.9	–	4.9	5.3	8.3
WM3	3	25	196.0	195.0	125.0	91.0	42.8	6.3	–	5.8	5.7	8.0

AP refers to the aperture of the TGMs. h_j refers to the hydraulic head of the i-th point; $\triangle h_{i-j}$ stands for the hydraulic head difference between the i-th point and the j-th point; "–" means that the local hydraulic head was beyond the measurement range of the piezometric tube or there was no TGM between the two points.

another key factor in the evaluation of the killing efficiency of the TGMs. The intensive layout improved the killing rates of the WMs perhaps because it increased the flow velocity of the water just passing the WMs (Fig. 7). In summary, TGMs with higher flow capacities and the ability to generate stronger turbulence should be chosen as the preferred materials if they do not substantially affect the economic efficiency.

4.5.3. Circular killing test

In the direct killing tests, water only passed through 25 TGMs and the killing rate might be further improved if the veligers were treated with more TGMs. Therefore, circular killing tests were operated to explore the killing potential of the TGMs. Since it was impossible to extend the experimental pipeline, the circulation of water in the existing facility was the only option to check whether the circulation time, the increase of which represented the increase of the number of TGMs, had effects on the killing rates.

The results demonstrated that the developmental stages and death modes in the circular killing tests were the same as those in direct killing tests. As shown in Fig. 15, the death rates of veligers all increased with the circulation time within the first 5 min and mostly stayed steady at over 70% beyond 5 min, which was in accordance with the results of the previous circular killing experiment (Xu, 2012). As the average flow velocity of the main flow approximated to 1 m/s, the circulated water volume flowed through the entire pipeline every 30 s. About 10 circulations was completed in 5 min, which is equivalent to treating the water body with 250 TGMs, and consequently, the killing effects were significantly improved. Therefore, the circular arrangement is convenient for an engineering environment with limited space but unlimited time. The death rates of the veligers were higher for the PP installation than that for the WM installation in the sparse layout while the difference was difficult to detect for the intensive layout. These results suggested that the intensive layout is preferred especially for WMs.

5. Discussion

5.1. The mechanism of killing veligers by turbulence

Based on the analysis described in Section 4.3.2, the existence of TGMs, especially the PPs, changes the turbulent energy of various frequencies. According to the Taylor's hypothesis of frozen turbulence (Taylor, 1938), the length scale of the turbulence decreases as the frequency increases under a constant convection velocity. The energy spectra illustrated that both the PP and WM installations resulted in an increase of the starting frequency of the inertial subrange, which led to the extension of the spectrum to a higher frequency and the insufficiency of the measurement range to demonstrate the entire inertial subrange. Since the inertial subrange is expected to follow an $f^{-5/3}$ slope according to the Kolmogorov law (Pope, 2000), the start at a higher frequency will result in the end at a higher frequency, which is also the starting point for the dissipation range. Therefore, the dissipation range will exhibit a higher frequency and a smaller length scale, even close to the Kolmogorov scale. Rehmann et al. (2003) made the hypothesis for the mortality of zebra mussel veligers that the shear forces generated by turbulence of the same length scale with Kolmogorov length could threaten the veligers, which was proven by the increase of veliger mortality when the Kolmogorov length became comparable or even shorter than the body lengths of the veligers. Because zebra mussels and golden mussels have many common or close

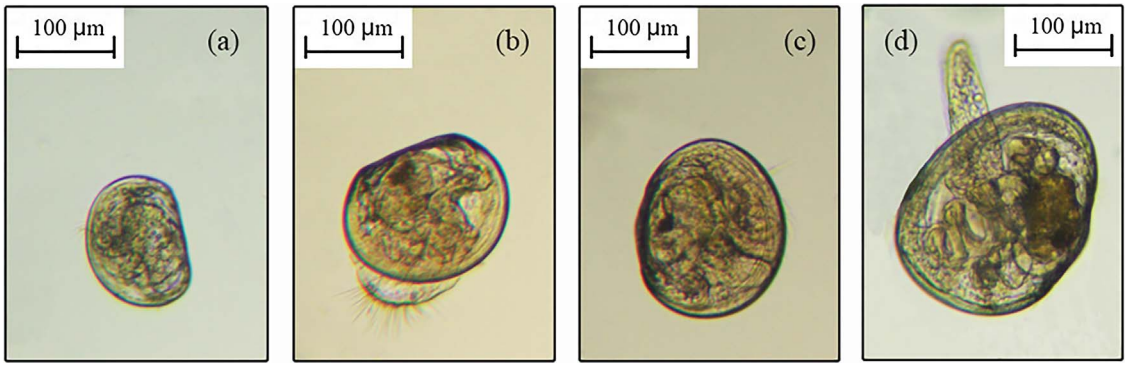

Fig. 12. Different plankton stages of golden mussel larvae in the water: (a) D-shape veliger; (b) Umboned veliger; (c) Pediveliger; and (d) Plantigrade veliger.

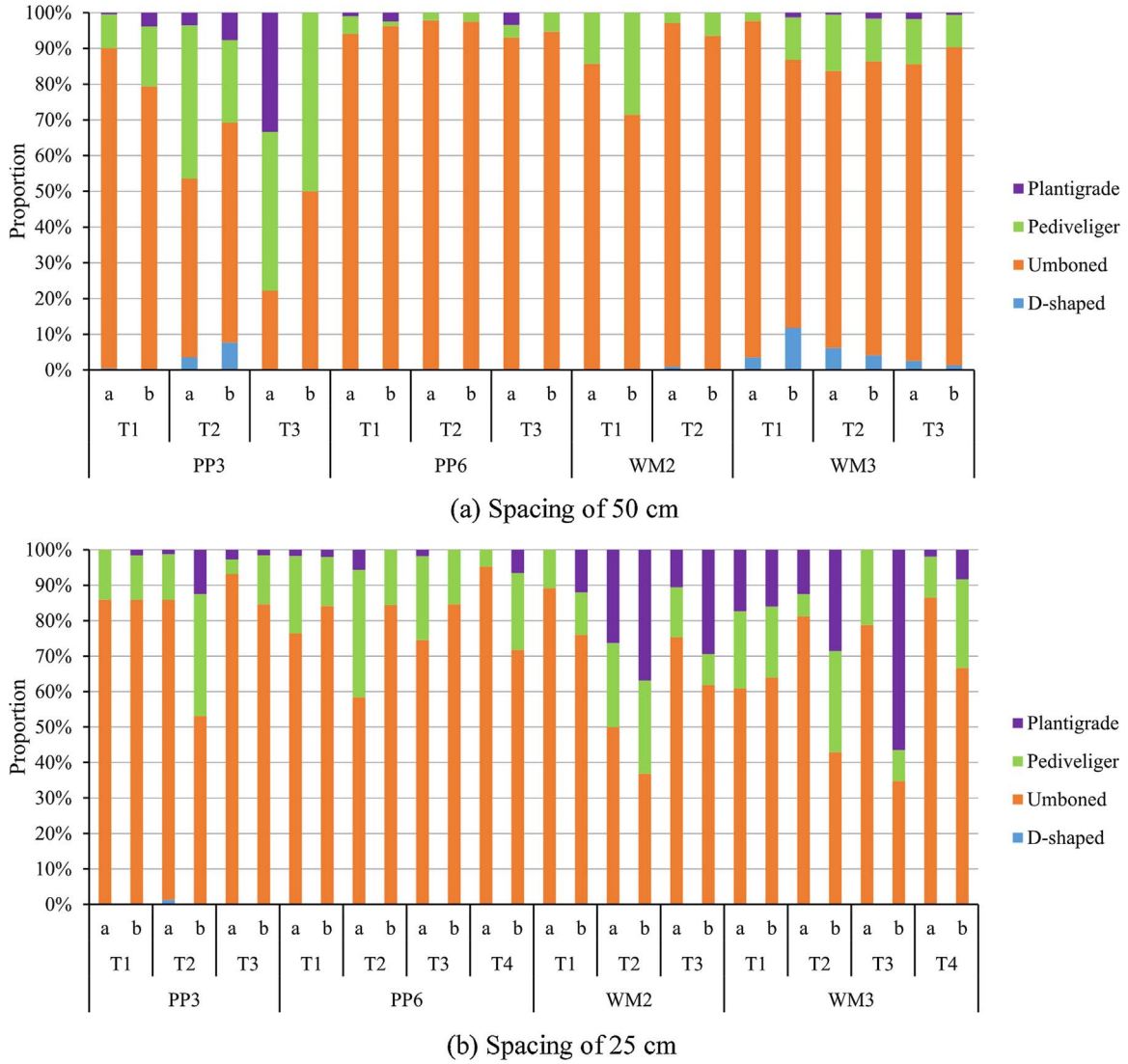

Fig. 13. Proportion of life stages of golden mussel larvae. "a" refers to the upstream sampling location and "b" refers to the downstream sampling location. Ti refers to the *i*-th test within the same TGM experiment.

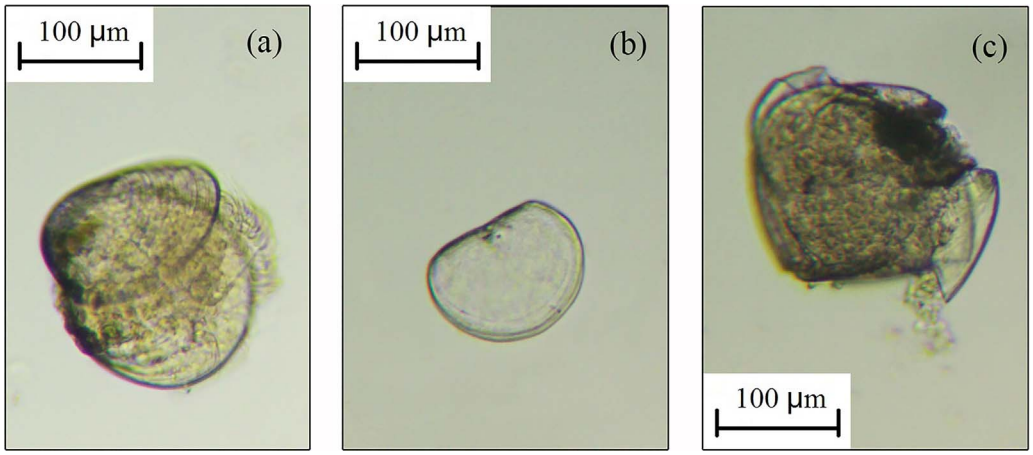

Fig. 14. Status of veligers after treatment with high frequency turbulence: (a) the tissues of the veliger were broken and released out from the shells; (b) empty shell due to the release of all the tissues; and (c) the shells of the veligers were damaged.

biological characteristics (Morton, 1979; Ricciardi, 1998; Karatayev et al., 2007), it is reasonable to explain the mechanism of the killing of golden mussel veligers using turbulence by the length scale of turbulence.

At the Kolmogorov scale, the viscous stress is comparable to the inertial process (Rehmann et al., 2003):

$$\mathrm{Re}_K = \frac{u_K l_K}{\nu} \approx 1 \tag{4}$$

where Re_K is the Reynolds number at the Kolmogorov length; u_K and l_K

Table 3
Death rates of golden mussel veligers in direct killing tests.

Spacing/cm	TGM	U_{mean1}/U_0	σ_{w1}/σ_0	Test	WT/°C	DR_0/%	DR_1/%	ΔDR/%
50	PP3	0.994	3.893	T1	23.8	19.39	46.31	26.92
				T2	23.8	66.67	91.56	24.89
				T3	25.0	35.71	45.45	9.74
	PP6	1.142	13.947	T1	24.0	24.06	33.61	9.55
				T2	24.0	33.33	63.30	29.97
				T3	24.0	25.64	64.15	38.51
	WM2	1.129	1.252	T1	24.0	30.00	46.15	16.15
				T2	24.0	46.91	52.31	5.40
	WM3	1.115	2.554	T1	24.0	36.09	37.87	1.78
				T2	24.0	25.21	36.22	11.01
				T3	24.0	20.81	38.25	17.44
25	PP3	0.884	2.983	T1	23.8	51.69	54.29	2.59
				T2	23.0	61.00	77.14	16.14
				T3	23.0	63.13	67.82	4.69
	PP6	1.043	11.376	T1	23.7	26.52	47.40	20.87
				T2	23.7	37.32	62.79	25.47
				T3	23.7	41.49	61.76	20.28
				T4	24.0	32.26	51.58	19.32
	WM2	1.163	1.354	T1	24.0	54.60	73.12	18.52
				T2	24.0	71.85	78.16	6.31
				T3	24.0	52.78	72.80	20.02
	WM3	1.076	2.597	T1	24.0	79.28	81.62	2.34
				T2	24.0	71.43	86.27	14.85
				T3	24.0	67.33	76.04	8.71
				T4	24.0	51.40	68.00	16.60

U_{mean1} and σ_{w1} refer to the arithmetic mean of the velocities measured in line V and the turbulence intensity of Z direction at the measuring section center at MD = 2.5 cm with the TGMs, respectively. WT is water temperature. Ti refers to the i-th test for the same TGM number. DR_0 is the death rate of golden mussel veligers at the sampling location "a", while DR_1 is the death rate at the sampling location "b". ΔDR equals to DR_1- DR_0, indicating the killing rate.

are the velocity scale and length scale in the Kolmogorov scale, respectively; and ν is the kinematic viscosity of water. The value for a temperature of 24 °C was taken as representative of the experiments listed in Table 3. The length scale l_K is defined as:

$$l_K = \left(\frac{\nu^3}{\varepsilon}\right)^{1/4} \tag{5}$$

where ε is the dissipation rate.

The ratio of the body length of the mussel veliger, d, and the Kolmogorov scale was defined by Rehmann et al. (2003) to quantitatively assess the influence of turbulence on veligers. The ratio is named as the relative body length in this study:

$$d^* = \frac{d}{l_K} \tag{6}$$

The length scale of the turbulent eddy was believed to be small enough to enhance the veliger mortality if $d^* \geq 1$ (Rehmann et al., 2003). However, the method for the dissipation rate by fitting the inertial subrange of the energy spectrum (Rehmann et al., 2003; Bluteau et al., 2011) was not applicable in this study because the measurements could not assess the entire inertial subrange. Therefore, the dissipation rate ε was calculated using the method of O'Connor et al. (2010), which does not require the determination of the entire inertial subrange in the spectrum:

$$\varepsilon = 2\pi\left(\frac{2}{3a}\right)^{3/2}\sigma_{\overline{V}}^3(L^{2/3} - L_1^{2/3})^{-3/2} \tag{7}$$

where a = 0.5 is the Kolmogorov constant (Sreenivasan, 1995); $\sigma_{\overline{V}}$ is the fluctuating velocity component; L (=NUt, U is the local flow velocity, and t = 1/200 s is the time interval) is the length scale over N intervals; and L_1 is the length scale for a single interval:

$$L_1 = Ut + 2z\sin(\frac{\theta}{2}) \tag{8}$$

where z is the height and θ is the half-angle divergence of the beam of the transmitted pulses. Since the distance between the transmitter of the ADV and the measuring point was only 5 cm, the divergence of the pulse beam can be ignored and then $\theta \approx 0$.

As shown in Section 4.5, the umboned veligers and pediveligers composed the overwhelming majority of the veligers in the test period, the characteristic body length of these two developmental stages is approximately 200 μm on average (the range of body length is between 180 and 220 μm). This value was applied in the calculation of d^*. The turbulence intensity in the Z direction was again utilized, therefore, $\sigma_{\overline{V}} = \sigma_w$. Combined with Eqs. (2) and (3), the distribution of d^* was calculated and is shown in Fig. 16.

For the PPs, the maximum of the downstream d^* approximated or exceeded 1, e.g., the downstream $(d^*)_{max}$ = 3.16 for PP6 (sparse layout). However, the $(d^*)_{max}$ was smaller than 1 for WM2($(d^*)_{max}$ = 0.48 with sparse layout) and approached 1 for WM3. Generally, the length scale of the turbulence for the PPs is smaller than that for the WMs, and, hence, the PPs theoretically have a stronger capacity for mussel veliger killing, which is consistent with the experimental results of the direct killing tests.

The distribution of d^* did not change noticeably when the intensive layout was applied (Fig. 16b) comparing with the sparse layout, while the value of d^* in the downstream area close to the TGMs experienced remarkable variation. For instance, the downstream $(d^*)_{max}$ for WM2 increased from 0.48 to 0.76, owing to the sharp acceleration of water flowing through the WMs; the downstream $(d^*)_{max}$ for PP3 dropped from 1.32 to 1.12, which might be the result of the decrease of the flow velocity due to the loss of flow capacity under the intensive layout. The examples above illustrate that $(d^*)_{max}$ reflects the influence of both the local flow velocity and the turbulence intensity downstream of the TGMs.

The contour lines of d^* were almost perpendicular to the flow direction in the main flow area after water just passed the TGMs, and, therefore, most water would pass the zone with the largest d^*, where the veligers might receive the most intensive killing treatment. Based on the foregoing statement, the relation between the killing rate and $(d^*)_{max}$ was examined and is displayed in Fig. 17.

In spite of fluctuations in the killing rates among the killing tests,

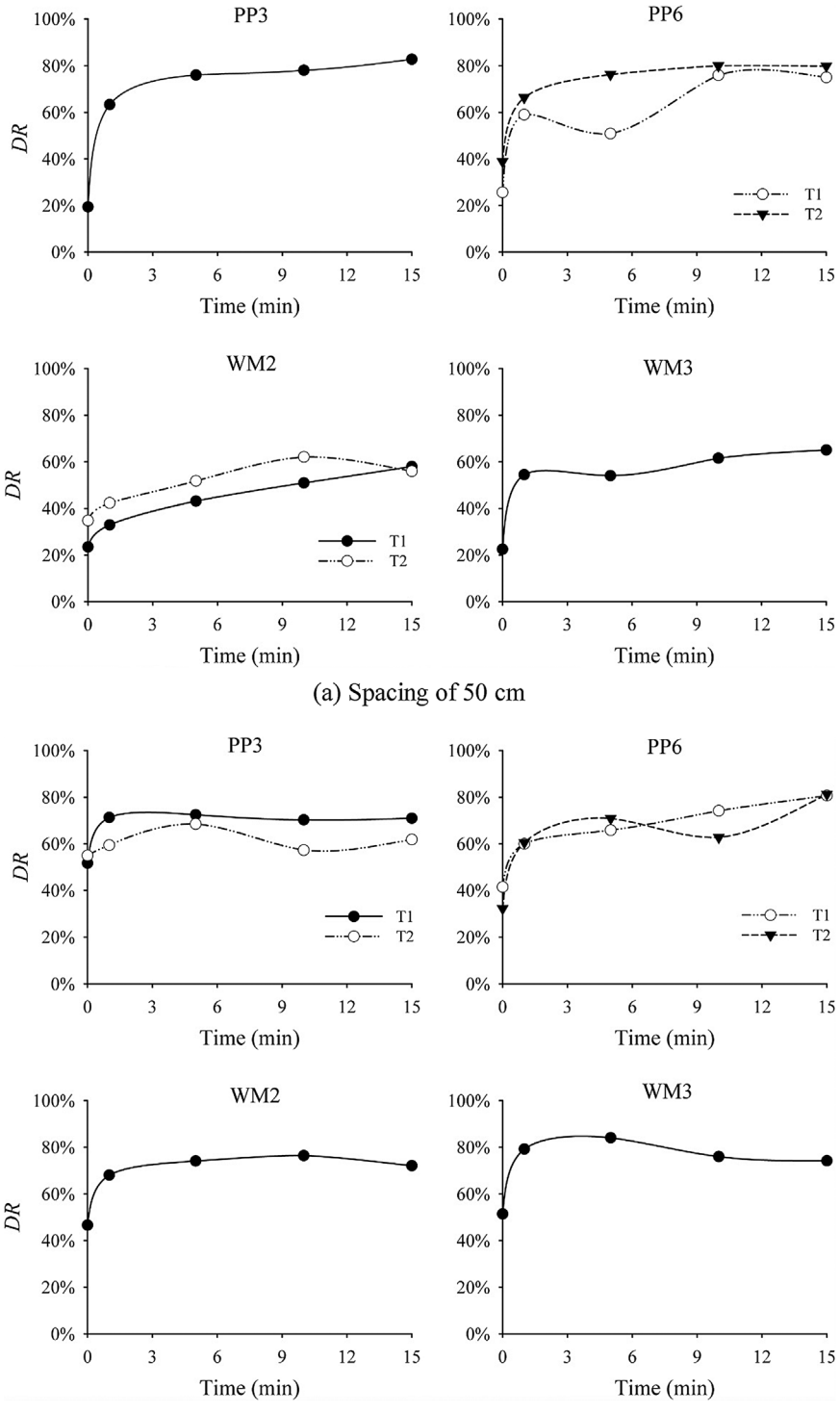

Fig. 15. Death rates of the circular killing tests: (a) Spacing of the TGMs was 50 cm; and (b) Spacing of the TGMs was 25 cm. The death rate at 0 min was the rate in the forebay.

there remains a clear trend that the killing rate increases as $(d^*)_{max}$ increases ($R^2 = 0.32$, $p = 0.003$, Fig. 17). This finding agrees with and even extends the conclusion of Rehmann et al. (2003). Only d^* ranging from 0 to 1.2 was inspected in the experiment by Rehmann et al. (2003) owing to the limitation of turbulence intensity generated by airflows. With a much larger range of $(d^*)_{max}$ in this study, the relation is still valid, suggesting that $(d^*)_{max}$ can be a reference index for the evaluation of killing effects of TGMs.

Specifically, the killing rate of the PPs exhibits an one-way increase with $(d^*)_{max}$, however, the trend is not so distinct for the WMs. $(d^*)_{max}$ of WM2 is smaller than that of WM3, but the killing rate is higher. It is probably because the killing rate only increases steadily with the growth of d^* if $d^* > 0.9$ (Rehmann et al., 2003). In this study, $(d^*)_{max} < 0.9$ for WM2 and $(d^*)_{max} \leq 1.0$ for WM3, therefore, the turbulence might not be strong enough to stabilize the killing effects. Combining the result of this study and the study of Rehmann et al. (2003), the criterion for steady killing is adjusted to $(d^*)_{max} > 1$. However, the size of the area with $(d^*)_{max} > 1$ could not be controlled in this study, therefore, the influence of $(d^*)_{max}$ on the killing rate remains to be explored by further research. The $(d^*)_{max}$ criterion is likely

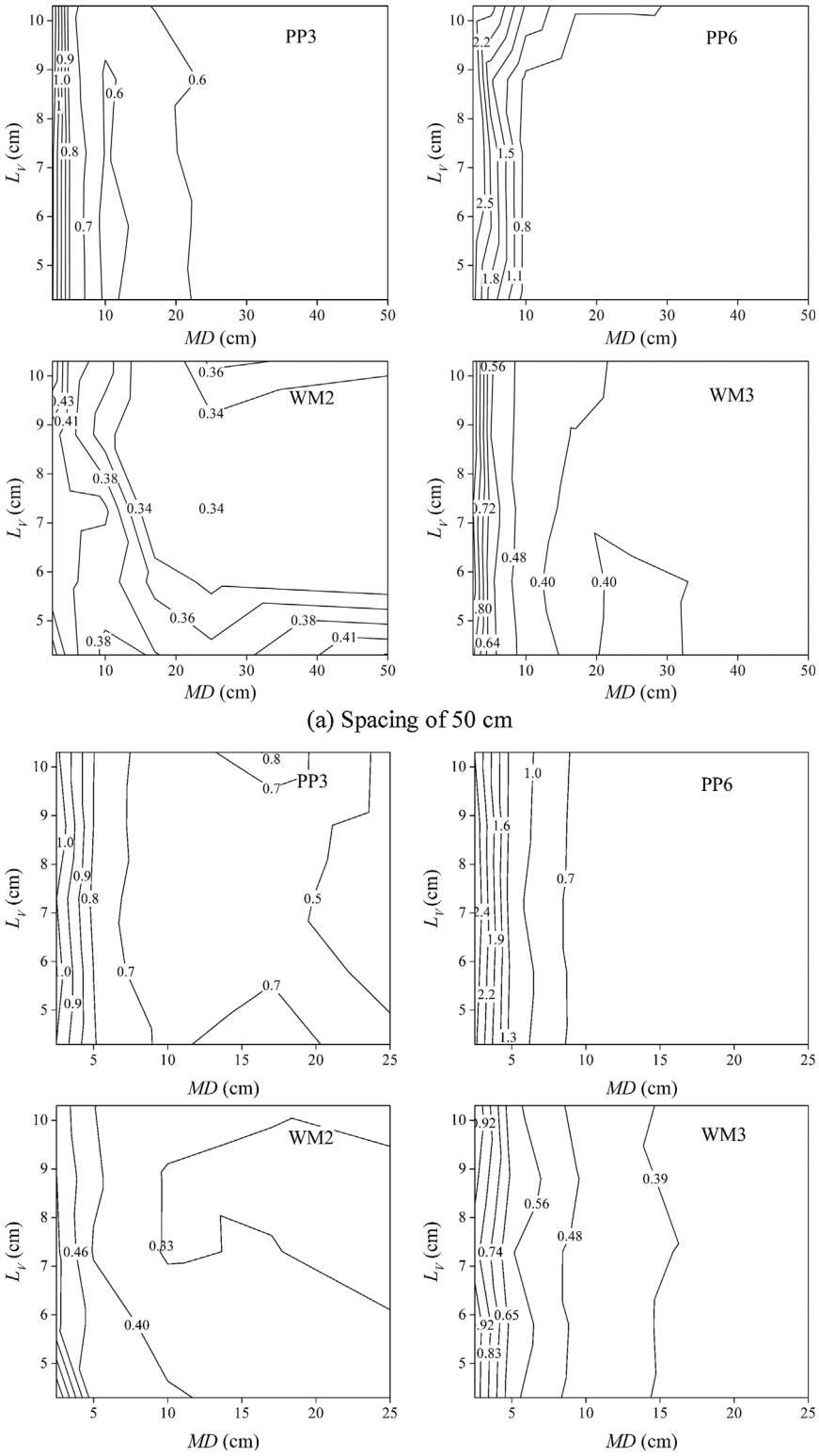

Fig. 16. Distribution of d^* when the interval of TGMs is (a) 50 cm and (b) 25 cm.

valid for all veligers regardless of their sizes considering that the critical value of d^* for zebra mussel veligers of different sizes remained unchanged in Rehmann et al. (2003). Thomas and Gibson (1990) described the force exerted by the turbulence on the veligers as:

$$\tau = \mu\left(\frac{\varepsilon}{\nu}\right)^{1/2} d^2 = \frac{\mu d^{*2}}{\nu} \quad (9)$$

where μ is the dynamic viscosity. If μ and ν stay constant, the force can only increase when $d^* > 1$, which is consistent with the criterion described in this paper.

5.2. Influence of the boundary layer

The turbulence intensity is generally strong in the boundary layer of

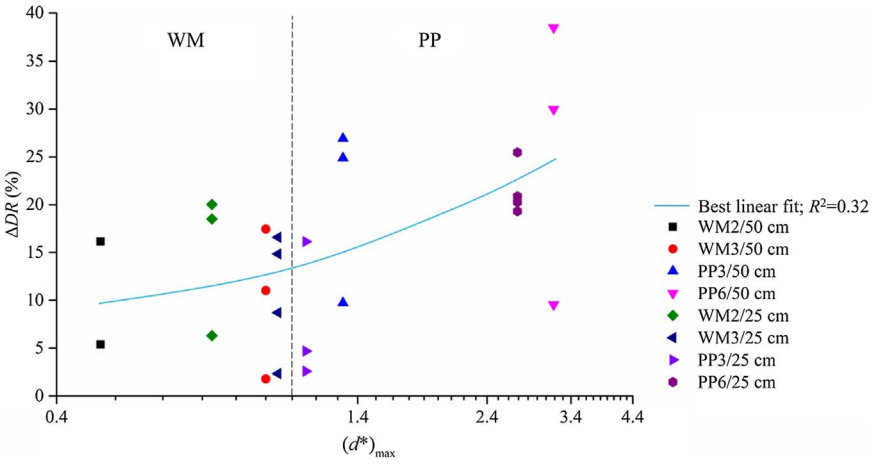

Fig. 17. Relation between the killing rate ΔDR and $(d^*)_{max}$.

a pipeline without TGMs (Schlichting et al., 2000). However, with the existence of the TGMs, the main flow area was largely affected and the turbulence intensity distribution was correspondingly changed. In most cases, the banded feature of the turbulence intensity and the d^* distribution suggested that the boundary layer effect could be ignored in the main flow area. However, the boundary layer effect for WM2 was so strong that the banded feature of the turbulence intensity was not noticeable (Figs. 9 and 16). Therefore, the influence of the boundary layer is discussed in this section with the measurements along line H, taking WM2 and PP6 installation (sparse layout) as examples.

As WM2 and PP6 yielded the lowest and highest turbulence intensity downstream, respectively, distinctive distributions of d^* were observed near the pipe wall. $(d^*)_{max}$ was 1.07 in the boundary layer for WM2, while $(d^*)_{max}$ was 3.16 near the pipe center for PP6. The gradient of d^* near the wall was greater than that in the main flow area for WM2 (Fig. 18a), and the greatest gradient of d^* was distributed in the banded zone for PP6 (Fig. 18b). The area affected by the boundary layer for WM2 was larger than that for PP6. In other words, the influence of the boundary layer is strong when the turbulence produced by the TGMs is weak, while it is negligible when the turbulence generated by the TGMs is intense. Although the influence of the boundary layer on the distribution of d^* for WM2 was not negligible, the zone showing significant impact was long but narrow, which was 0.5–0.8 cm wide as shown in Fig. 18a. The discharge passing this area only took up about 10% of the total flow. Hence, the actual influence from the boundary layer to veliger killing was limited assuming that the veligers were distributed evenly in the water. For PP6, the boundary layer was unnoticeable in the zone downstream at $MD < 10$ cm, where the values of d^* were large (Fig. 18b). The veligers might receive similar treatment of turbulence in both the boundary layer and the main flow area after they passed through the TGM, thus, the influence of boundary layer could be ruled out.

5.3. Application of TGMs

When the TGMs are applied in the cooling pipelines for the prevention of golden mussel fouling, they can be installed directly in the pipelines like the installation in the experiments. If it is not feasible to install the TGMs in the cooling pipelines directly, the TGMs can also be managed in an extension pipeline connecting to the cooling system to treat water before it enters into the cooling pipelines. In either installation method, to ensure the proper functioning of the TGMs, a mesh filter is required to prevent suspended matters from entering the pipeline system and clogging the apertures of the TGMs. In the Langyashan PSP, a 300 μm-aperture strainer and a 50 μm-aperture strainer were installed at the entrance of the cooling system to filter the suspended matters, thus, the tested TGMs will function well if installed in the cooling pipelines in the Langyashan PSP.

Another issue about TGM application in the cooling system is that the potential influence to other planktons in the water. Since the macro-planktons would be blocked by the filter, only the micro-planktons with similar and smaller sizes as golden mussel veligers could enter the cooling pipeline. Peters and Marrasé (2000) summarized the effect of turbulence on planktons: in general, turbulence has negative effect on

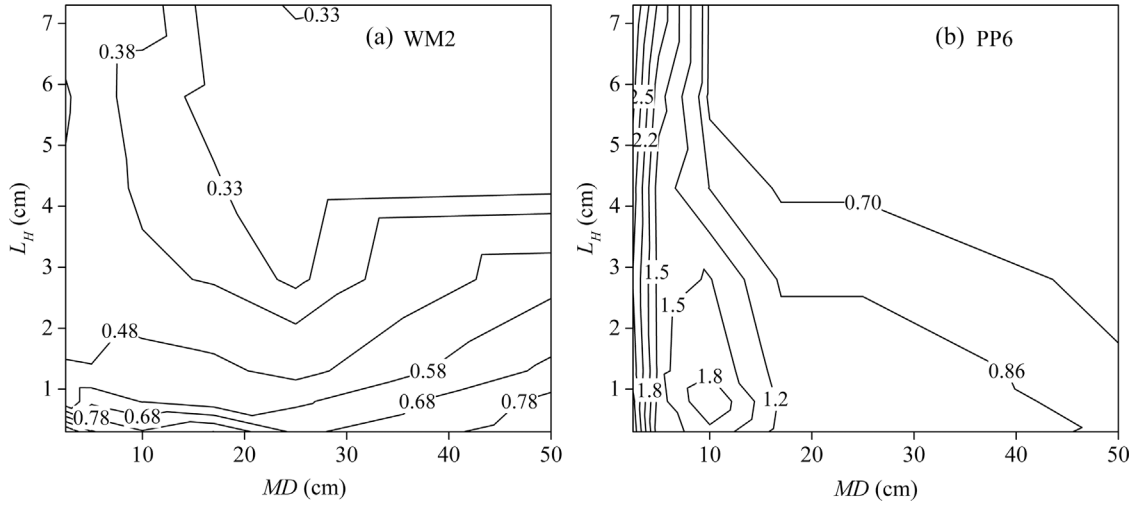

Fig. 18. Distribution of d^* for (a) WM2 and (b) PP6 for the layout with the spacing of 50 cm.

growth rates of planktons, increases energy expenditures, and improves ingestion rates, especially at low and moderate turbulence intensities. Planktonic organisms larger than the turbulent eddies at Kolmogorov length scale will be affected by the turbulent shear forces directly (Zhou et al., 2016), which would weaken the ability of the organisms in detecting or capturing food, and would also cause injuries to the larger organisms (Visser et al., 2009). Therefore, it is reasonable to infer a general suppressing effect from the TGM installation to the planktons that have similar sizes with the golden mussel veligers in the cooling pipelines. While effectiveness of the turbulences on different organisms may be different to a large extent (Jessopp, 2007). The planktons, which have much smaller sizes than the golden mussel veligers, are hardly susceptible to the influence of the TGM installation designed for golden mussel veligers, because the calculated $(d^*)_{max}$ according to the smaller body length is smaller than 1. So the influence of the TGMs on the micro-planktons can be ignored.

6. Conclusion

The number of TGMs had little influence on the downstream distribution of the main flow velocity component, and the magnitude and energy spectrum of the turbulence intensity when the number of TGMs reached 3 for the sparse layout and 5 for the intensive layout. A spatially short fluctuation of flow velocity emerged immediately after the water passed a TGM. The fluctuation lasted only a short distance longitudinally and then the water returned to a similar status as without TGMs. For the PPs, the transverse variance of the velocity distribution was enlarged. The velocity magnitude was increased after passing the PPs with large aperture while it decreased after passing the PPs with small aperture. For the WMs, the magnitude of the downstream velocity close to the materials was improved, regardless of the aperture size. The intensive layout produced a more uniform transverse distribution of flow velocity downstream of the PPs with large pores and a sharp increase of flow velocity downstream of the WMs.

The highest turbulence intensity was distributed in a 3 cm-long longitudinal zone downstream of the TGMs and then decreased rapidly to a stable value. The distribution of turbulence intensity showed a distinct banded feature for most tested TGMs. The maximum of the turbulence intensity increased with the apertures of the PPs. Both the PPs and WMs were capable of improving the starting frequency of the inertial subrange in the energy spectrum, and, thus, reducing the length scale of the dissipation range.

Results of the killing tests demonstrated similar death modes of golden mussel veligers as for zebra mussels in previous experiments (Rehmann et al., 2003) in which high-frequency turbulence was generated by aerating pumps. Therefore, similar killing mechanisms were assumed, i.e. when the dissipation ranges of turbulent eddies had length scales similar to the body lengths of the mussel veligers, shear stress generated by the eddies would damage the veligers. The hypothesis was then proved by the positive relation between the killing rate and $(d^*)_{max}$, where $(d^*)_{max}$ is a representative index of the hydraulic characteristics which combines the effects of both local flow velocity and turbulence intensity. Therefore, $(d^*)_{max}$ is recommended as an indicator of the killing effect of various turbulence-generating methods. $(d^*)_{max} > 1$ is set as the criterion that a TGM has a high and steady killing capacity.

Circular tests, which simulated the elongation of the experimental pipeline and increase of effective number of TGMs, were conducted to explore the effect of treatment time on veliger killing. The mortality rate of the veligers was significantly enhanced within the first 5 min and then stayed constant. Circulation is, therefore, recommended for engineering projects with limited space but less limits on time.

The ranking of hydraulic head loss for the tested TGMs was PP3 > PP6 > WM3 > WM2. The intensive layout did not substantially increase the hydraulic head loss for the TGMs, thus, only the number of TGMs affected the total head loss. With comprehensive considerations of the killing capacity and economic efficiency, PP6 with the sparse layout is recommended as the TGM for the control of golden mussel veligers. If WMs are selected as the TGMs owing to their outstanding flow capacity, the intensive layout should be used.

Acknowledgements

This study was supported by the Natural Science Foundation of China (51479091, 51409146), the Construction and Administration Bureau of South to North Water Diversion Middle Route Project (ZXJ/YW/JF-017), Tsinghua University Project (20151080440), and the State Key Laboratory of Hydroscience and Engineering project (2016-KY-04). We would like to thank the reviewers and editors for their comments that help improve the manuscript. We also thank Professor C. S. Melching for revising the language.

References

Bluteau, C.E., Jones, N.L., Ivey, G.N., 2011. Estimating turbulent kinetic energy dissipation using the inertial subrange method in environmental flows. Limnol. Oceanogr.: Methods 9, 302–321.
Cataldo, D.H., 2015. Larval development of *Limnoperna Fortunei*. *Limnoperna Fortunei*. Springer International Publishing, pp. 43–53.
Chanson, H., Trevethan, M., Koch, C., 2007. Discussion of 'Turbulence measurements with acoustic Doppler velocimeters' by Carlos M. García, Mariano I. Cantero, Yarko Niño, and Marcelo H. García. J. Hydraul. Eng. 133 (11), 1283–1286.
Darrigran, G., Damborenea, C., Greco, N., 2007. Freshwater invasive bivalves in man-made environments: a case study of larvae biology of *Limnoperna fortunei* in a hydroelectric power plant in South America. AMBIO 36 (7), 575–579.
Darrigran, G., Damborenea, C., Drago, E., Ezcurra de Drago, I., Paira, A., 2011. Environmental factors restrict the invasion process of Limnoperna fortunei (Mytilidae) in the Neotropical Region: a case study from the Andean tributaries. Ann. Limnol. 47 (3), 221–229.
Darrigran, G., Damborenea, C., Drago, E., Ezcurra de Drago, I., Paira, A., Archuby, F., 2012. Invasion process of *Limnoperna fortunei* (Bivalvia, Mytilidae): the case of Uruguay River and emissaries of the Iberá Wetland, Argentina. Zoologia 29 (6), 531–539.
Darrigran, G., 2002. Potential impact of filter-feeding invaders on temperate inland freshwater environments. Biol. Invasions 4 (1–2), 145–156.
Dunker, W., 1856. Mytilacea nova collectionis cumingiana. Proc. Zool. Soc. Lond. 24, 358–366.
Fushoku, B., Bumon, I., 1999. Adhesion mechanism of marine sessile animals and anti-fouling counter measure. Nippon Zairyo Gakkai 213, 44–53.
Garcia, C.M., Mariano, I.C., Nino, Y., Garcia, M.H., 2005. Turbulence measurements with acoustic Doppler velocimeters. J. Hydraul. Eng. 131 (12), 1062–1073.
Goring, D.G., Nikora, V.I., 2002. Despiking acoustic Doppler velocimeter data. J. Hydraul. Eng. 128 (1), 117–126.
Group of Pipeline Study, the Chinese academy of sciences institute of aquatic organisms, 1973. Biology of golden mussel (*Limnoperna fortunei*). Anim. Prev. 42, 33–36 (in Chinese with English abstract).
Horvath, T.G., Lamberti, G.A., 1999. Mortality of zebra mussel, *Dreissena polymorpha*, veligers during downstream transport. Freshwater Biol. 42, 69–76.
Hussein, H.J., Capp, S.P., George, W.K., 1994. Velocity measurements in a high-Reynolds-number momentum-conserving, axisymmetrical, turbulent jet. J. Fluid Mech. 258, 31–75.
Jessopp, M.J., 2007. The quick and the dead: larval mortality due to turbulent tidal transport. J. Mar. Biol. Assoc. U. K. 87 (03), 675–680.
Karatayev, A., Boltovskoy, D., Padilla, D., Burlakova, L., 2007. The invasive bivalves Dreissena polymorpha and *Limnoperna fortunei*: parallels, contrasts, potential spread and invasion impacts. J. Shellfish Res. 26 (1), 205–213.
Liu, Y.Y., Zhang, W.Z., Wang, Y.X., 1979. China's Economic Animal Annals (Freshwater Molluscs). Science Press, Beijing, China (in Chinese with English abstract).
Lohrmann, A., Cabrera, R., Kraus, N.C., 1994. Acoustic Doppler velocimeter (ADV) for laboratory use. In: Pugh, C.A. (Ed.), Proc., Symp. on Fundamentals and Advancements in Hydraulic Measurements and Experimentation. ASCE, Reston, VA, pp. 351–365.
McEnnulty, F.R., Bax, N.J., Schaffelke, B., Campbell, M.L., 2001. A Review of Rapid Response Options for the Control of ABWMAC Listed Introduced Marine Pest Species and Related Taxa in Australian Waters. Technical Report No. 23. Centre for Research on Introduced Marine Pests, CSIRO Marine Research, Hobart.
Mohamed, M.S., LaRue, J.C., 1990. The decay power law in grid-generated turbulence. J. Fluid Mech. 219, 195–214.
Montalto, L., Rojas Molina, F., 2014. Byssal hairs in the invasive Asian freshwater bivalve *Limnoperna fortunei* (Mytilidae) in the Paraná River system with comments on this species in South America. Molluscan Res. 34, 127–138.
Morton, B., 1977. The population dynamics of *Limnoperna fortunei* (Dunker 1857) (Bivalva: Mytilacea) in Plover Cove reservoir, Hong Kong. Malacologia 16, 165–182.
Morton, B., 1979. Freshwater fouling bivalves. Proceedings of the First International Corbicula Symposium. Texas Christian University, Fort Worth, Texas.
O'Connor, E.J., Illingworth, A.J., Brooks, I.M., Westbrook, C.D., Hogan, R.J., Davies, F.,

Brooks, B.J., 2010. A method for estimating the turbulent kinetic energy dissipation rate from a vertically pointing Doppler lidar, and independent evaluation from balloon-borne in situ measurements. J. Atmos. Ocean. Technol. 27 (10), 1652–1664.
Pereyra, P.J., Bulus Rossini, G., Darrigran, G., 2011. Toxicity of three commercial tannins to the nuisance invasive species *Limnoperna fortunei* (Dunker, 1857): implications for control. Fresenius Environ. Bull. 20 (6), 1432–1437.
Pereyra, P.J., Bulus Rossini, G., Darrigran, G., 2012. Toxicity of Neem's oil, a potential biocide against the invasive mussel *Limnoperna fortunei* (Dunker, 1857). An. Acad. Bras. Ciênc 84 (4), 1065–1071.
Perez, M., Garcia, M., Traversa, L., Stupak, M., 2003. Concrete deterioration by golden mussels. In: Conference on Microbial Impact on Building Materials. 8–9 September 2003, Lisbon, Portugal.
Peters, F., Marrasé, C., 2000. Effects of turbulence on plankton: an overview of experimental evidence and some theoretical considerations. Mar. Ecol. Prog. Ser. 205, 291–306.
Pope, S.B., 2000. Turbulent Flows. Cambridge University Press.
Rehmann, C.R., Stoeckel, J.A., Schneider, D.W., 2003. Effect of turbulence on the mortality of zebra mussel veligers. Can. J. Zool. 81, 1063–1069.
Ricciardi, A., 1998. Global range expansion of the Asian mussel *Limnoperna fortunei* (Mytilidae): another fouling threat to freshwater systems. Biofouling 13 (2), 97–106.
Rusello, P.J., Lohrmann, A., Siegel, E., Maddux, T., 2006. Improvements in acoustic Doppler velocimetery. In: The Seventh International Conference on Hydroscience and Engineering. September 10–13, 2006, Philadelphia, Pennsylvania.
Schlichting, H., Gersten, K., Gersten, K., 2000. Boundary-Layer Theory. Springer Science & Business Media.
Sreenivasan, K.R., 1995. On the universality of the Kolmogorov constant. Phys. Fluids 7, 2778–2784.
Taylor, G.I., 1938. The spectrum of turbulence. Proc. R. Soc. A 164, 476–490.
Thomas, W.H., Gibson, C.H., 1990. Quantified small-scale turbulence inhibits a red tide dinoflagellate, Gonyaulax polyedra Stein. Deep-Sea Res. 37, 1583–1593.
Visser, A.W., Mariani, P., Pigolotti, S., 2009. Swimming in turbulence: zooplankton fitness in terms of foraging efficiency and predation risk. J. Plankton Res. 121–133.
Voulgaris, G., Trowbridge, J.H., 1998. Evaluation of the acoustic Doppler velocimeter (ADV) for turbulence measurements. J. Atmos. Ocean. Technol. 15 (1), 272–289.
Welch, P.D., 1967. The use of fast fourier transform for the estimation of power spectra: a method based on time averaging over short, modified periodograms. IEEE Trans. Audio Electroacoust. AU-15, 70–73.
Xu, M.Z., Wang, Z.Y., Duan, X.H., Zhuang, M.Q., de Souza, F.T., 2009. Ecological measures of controlling invasion of golden mussel (*Limnoperna fortunei*) in water transfer systems. In: 33rd IAHR Congress: Water Engineering for a Sustainable Environment. International Association of Hydraulic Engineering and Research. pp. 1609–1616.
Xu, M.Z., Cao, X.W., Wang, Z.Y., Wang, X.Z., 2012. Attachment characteristics of golden mussels (*Limnoperna fortunei*) in water transport projects. J. Tsinghua Univ. (Sci. & Techol.) 52 (2), 170–176.
Xu, M.Z., Darrigran, G., Wang, Z.Y., Zhao, N., Lin, C.C., Pan, B.Z., 2015a. Experimental study on control of *Limnoperna fortunei* biofouling in water transfer tunnels. J. Hydro-Environ. Res. 9 (2), 248–258.
Xu, M.Z., Wang, Z.Y., Zhao, N., Pan, B.Z., 2015b. Growth, reproduction, and attachment of the golden mussel (*Limnoperna fortunei*) in water diversion projects. Acta Ecol. Sin. 35, 70–75.
Xu, M.Z., 2012. Experimental Study of Macroinvertebrate *Limnoperna Fortunei* Invasion and Prevention in Water Transfer Tunnels. Ph.D Thesis. Tsinghua University, Beijing (in Chinese with English abstract).
Xu, M.Z., 2013. Experimental study of biofouling control of *Limnoperna fortunei* in water transfer tunnels. Proceedings of 2013 IAHR Congress. Tsinghua University Press, Beijing.
Yan, J., Tang, H.W., Cheng, N.S., Zhou, Y.L., 2005. Review on study of vibrating grid turbulence and its application. Shuili Xuebao 36 (12), 1503–1509 (in Chinese with English abstract).
Ye, B.M., Cao, X.W., Xu, M.Z., Wang, Z.Y., Lin, C.C., 2011. Study of *Limnoperna fortunei* invasion in water transport project. Water Wastewater Eng. 37, 99–102 (in Chinese with English abstract).
Zhou, J., Han, X., Qin, B., Casenave, C., Yang, G., 2016. Response of zooplankton community to turbulence in large, shallow Lake Taihu: a mesocosm experiment. Fund Appl. Limnol. 187 (4). http://dx.doi.org/10.1127/fal/2016/0797.